Journal Pre-proof

Detection of Triacetone Triperoxide in air combining SnO_2 sensor e-nose enhanced with a kinetic model.

Raúl López, Marisol Vega, Luis M. Debán, Rafael Pardo

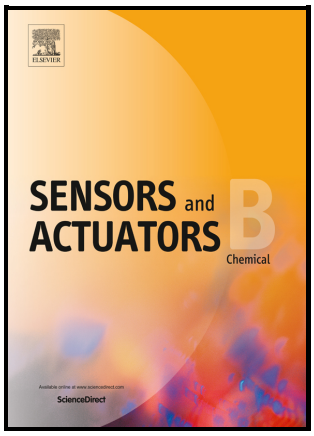

PII: S0925-4005(23)01960-3

DOI: https://doi.org/10.1016/j.snb.2023.135242

Reference: SNB135242

To appear in: *Sensors and Actuators: B. Chemical*

Received date: 14 October 2023
Revised date: 1 December 2023
Accepted date: 25 December 2023

Please cite this article as: Raúl López, Marisol Vega, Luis M. Debán and Rafael Pardo, Detection of Triacetone Triperoxide in air combining SnO_2 sensor e-nose enhanced with a kinetic model., *Sensors and Actuators: B. Chemical,* (2023) doi:https://doi.org/10.1016/j.snb.2023.135242

Detection of Triacetone Triperoxide in air combining SnO_2 sensor e-nose enhanced with a kinetic model.

Raúl López [a,b,1], Marisol Vega [a,c], Luis M. Debán [a], Rafael Pardo [a]

[a] *Department of Analytical Chemistry, Faculty of Sciences, Campus Miguel Delibes, University of Valladolid (Uva), Paseo Belén 7, 47011 Valladolid, Spain*
[b] *Department of Optoelectronics, Instituto Nacional de Técnica Aeroespacial (INTA), Ctra M301 km 10.5 edif 8, San Martín de la Vega, 28330, Madrid, Spain.*
[c] *Institute of Sustainable Processes (ISP), University of Valladolid, calle Dr. Mergelina s/n, 47011 Valladolid, Spain*

Abstract

In the domain of high-temperature semiconductor arrays for electronic noses (e-noses), Metal Oxide Sensors (MOS) have a pivotal role despite their non-linear response to chemical vapors. A prevalent approach to enhance the identification algorithm's performance involves implementing mathematical models during the MOS signal processing. However, certain models rely solely on mathematical goodness-of-fit, overlooking crucial features that render practical e-nose applications ineffective. This paper introduces a theoretical model for the qualitative analysis of MOS signals, focusing on two primary diffusion processes: analyte migration to the sensor's surface and the subsequent dispersion of some of these molecules within the MOS bulk. Additionally, this work discusses a model validation using an ad-hoc e-nose, built with SnO_2 gas sensors, and six organic chemicals, detailing main data processing steps. Finally, disclosed results showcase a high success rate for Triacetone Triperoxide (TATP) identification, one of the most significant threats among homemade explosives (HME). The presented conclusions underscore the enhanced efficacy of the proposed signal model for e-nose vapors identification and its practical utility in strengthening pre-emptive HME identification to enhance public safety.

Keywords: e-nose, tin oxide, gas sensor, Triacetone Triperoxide, homemade explosives, principal component analysis.

[1] Corresponding author.
Email address: lopezsr@inta.es (Raúl López Sánchez)

1. Introduction

Forensic analysis of airborne explosives remains critical for public safety and national security, given the increased use of improvised explosive devices (IEDs) in key public areas [1–4]. Although portable explosive vapor detectors (EVDs) have significatively evolved [5]. Frequently high false positive rates undermine their reliability, especially for homemade explosives (HMEs) [6] in non-contact detection scenarios, as many of HME have low vapor pressures [3,7,8] or insufficient olfactory signals [5], underscoring the need for dependable vapor-based identification technologies. A notable HME is Triacetone Triperoxide (TATP), often chosen for illicit activities due to its inexpensive and accessible ingredients [3,4,9]. This peroxide explosive, with no substantial legal uses [10], is alarmingly unstable yet highly powerful [2,9]. Conventional detection methods, like ultraviolet absorption or ionization, falter with TATP because of its nitro-group-free structure [2]. However, its high vapor pressure at ambient temperatures presents a distinctive avenue for detection through its emitted vapors [3,5].

[Fig. 1 about here.]

On-site explosive detection has historically faced challenges, resulting in continued reliance on sentinel species like trained canines [5], despite ongoing efforts to expand the use of chemical EVDs [6]. Comparatively, dogs exhibit exceptional olfactory sensitivity and instant response times [5,8] but are prone to fatigue and variability response in base of the type of training and scenario [5]. Conversely, explosive EVDs encompass a spectrum of tools from handheld units to substantial stationary systems, providing more reproducible results and facing fewer legal objections [5], being prominent technologies in explosive detection the ion mobility spectrometry (IMS) [1,6,11] and mass spectrometry (MS) [4,11,12]. Nonetheless, they suffer from some drawbacks including delayed responses (i.e., mainly due the separation technique to be coupled such as GC or HPLC), frequent false positives [5], and vulnerability to environmental pollutants [6]. Due to the constraints of traditional EVD techniques, electronic noses (e-noses) offer a compact detection alternative for explosive vapor analysis mirroring the mammalian olfactory mechanism and being able to discern chemical odor profiles through a sensor array [2,4,10]. Despite their utility in environmental surveillance and food integrity assessments [4,13], e-noses haven't gained prominence in HME detection due

to challenges in real-time correlation of vapors with their physical counterparts [4]. For instance, military-grade explosives detection (see Fig. 2), including when taggants are considered [3], demands detection thresholds in the parts-per-billion range [8].

[Fig. 2 about here.]

On the other side, HMEs, are simpler mixtures of chemicals and exhibit higher vapor pressures, highlight e-noses as promising alternative to EVDs for airborne identification [8] due their real-time functionality, enhanced portability, and precision. A standard portable e-nose is usually configured employing any of the following three sensor types [10]: metal oxide semiconductors (MOS) [14,15], quartz crystal microbalance (QCM), and surface acoustic wave (SAW) devices [16], looking for a balance between individual sensor sensitivity and array-wide selectivity to augment vapor discrimination capabilities [17]. Additionally, is common to enhance e-nose selectivity through signal preprocessing and extraction of fitting parameters from models (features) [17], followed by employing pattern recognition chemometrics (PARC) or machine learning techniques [8,10,12,13].

Doped tin oxide (SnO_2) is a prevalent MOS gas sensor, recognized for its semiconducting properties and sensitivity to certain HMEs [2,15], though it suffers from selectivity limitations when used independently [17,18], set in array show promising characteristics. Its chemiresistive response hinges on the analyte vapor molecules' interaction with surface adsorption [17,19], influenced by factors like oxygen vacancy sites, the Schottky barrier [2,14,19], vapor flow profile, inter alia [10]. These aspects alter the material's electrical resistivity, triggering a time-variant signal due to redox reactions between atmospheric oxygen, surface adsorbed, and analyte molecules [14,15,17]. However, practical application of MOS in vapor identification necessitates overcoming challenges like its nonlinear response to concentration [17] and control circuitry-induced shifts. In this manuscript, sensor responses are modeled in non-saturated SnO_2 response with a steady input function, dividing the signal into two primary temporal phases: an initial transitory regime (TR) where a time-sensitive gas signal is observed [19], akin to a capacitor's charging process (i.e., resistive-capacitive, RC, model, see Fig. 3), and a subsequent stationary region (SR) with a consistent response [13,14] despite the improvement that, conceptually, the RC model involved for MOS data analysis, from a practical point is not widely employed to perform a vapor identification because their

features (e.g., mainly τ) are strongly influenced by concentration and also the stage of the signal considered (i.e., τ reflects different quantitative results depending on the fraction of TR considered which, for practical purposes a signal qualitative analysis that employ RC model in an early TR region -1τ to 2τ- will carry to a totally different identification than those based on later TR regions -3τ to 4τ-).

[Fig. 3 about here.]

The literature offers various MOS response models [14,15,17–20], with several concentrating on operational facets (e.g., temperature effects) rather than vapor identification, limiting their applicability [19,20]. Others draw parallels between time-series data and mathematical functions like power-law [14,20], logarithmic models [17,18], or RC constructs [19]. However, when fitting is unfeasible, the signal complexity often yields oversimplification or misinterpretation, diminishing feature representativity and algorithmic precision. Therefore, to enhance response models, particularly for specific substances, could sharpen accuracy, minimize noise, and optimize ulterior PARC performance, although environmental conditions (e.g., humidity) may continue affecting to sensors and, therefore, ulterior vapor identification. Despite its importance, scant research exists on using e-noses for practical HME odor profiling [3], as most studies target smaller molecules with extensive sensor arrays [8], necessitating Neural Networks due to non-linear responses [8,13]. This manuscript proposes an innovative fitting model for the analysis of the MOS signals into Transitory Region, providing main features (i.e., variables) with relevant information about chemical vapor nature and minimizing the effect of concentration, especially useful for the identification of chemical vapors. Therefore, no derivative methodologies were required when chemical vapor identification is performed, and quantitative information is remained in MOS signal. Addressing this, our study confronts the complex identification of molecules like TATP [15] using a three-sensor e-nose, supplemented by a novel MOS diffusion model focused on analyte atmospheric-to-sensor surface migration and internal MOS diffusion with a validation across various chemicals, is then applied to TATP detection via PARC methodologies.

2. MOS response model and features

The SnO_2 sensors, when exposed to a constant concentration show a progressive conductance response shift with two differentiated zones: TR and SR. A response model for TR is proposed, analyzing sensor geometry and two diffusion processes: vapor circulation from atmosphere to the sensor surface and subsequent analyte diffusion into the bulk [15] (see Fig. 4).

[Fig. 4 about here.]

2.1. Analyte diffusion to the sensor surface

When analyte, A, is forced to enter the sensor chamber by inlet flow, q_i, it produces a vapor diffusion and a sensor response that can be mathematically modeled considering a dynamic interplay of two slow processes. Initially, the vapor of analyte reaches the sensor surface (see Fig. 4-a) and A initiates diffusion into the bulk (see Fig. 4-b) until a constant profile is reached according to Fick's law [21]. Both processes have concentration gradient as impulsive force. The first diffusion requires that A overcomes the sensor's boundary layer (i.e., a pseudo sphere with radius h in Fig. 4) to being surface chemisorpted and redox react with the adsorbed oxygen. Therefore, that first stage can be formulated by differential equation 2 and 2.

$$V^{-1}\frac{dh(t)}{dt} = q_i - q_o \qquad 1$$

$$V^{-1}\frac{dh(t)}{dt} = k_1 H(t-\theta)\alpha(t-\theta) - k_2 h(t) \qquad 2$$

Where q_i and q_o are the inlet and outlet flow rates, respectively, expressed in concentration units $[g \cdot L^{-1} \cdot s^{-1}]$, k_1 and k_2 are the inlet and outlet valve constants, respectively, V^{-1} represents reciprocal volume, and $dh(t)\ /\ dt$ is the variation of the amount of substance per unit of time in the sensor's boundary layer volume, α is the inlet total analyte amount of mass, θ is the delay of analyte to reach detector surface, H is Heaviside function and $h(t)$ is the amount of analyte available for the sensor to react. A known solution for equation 2, by a Laplace transform, is equation 3.

$$\frac{H(s)}{\alpha(s)} = \frac{K}{\tau \cdot s + 1} e^{-\theta s} \quad (3)$$

where $H(s)$, $\alpha(s)$ and s are the system response, the inlet amount of analyte and the complex variable, respectively, in the Laplace transform space, K is a variable that group constants, named static gain of the system, and τ is the time constant of the system. To simplify the model and adapt it to MOS responses for a step function, $\alpha(s) = m \,/\, s$, an inlet mass of m (i.e., $\alpha(t) = m$) can be assumed. Therefore, equation 3 can now solved $C_{A(0,t)}$ (i.e., the concentration of analyte A available for sensor surface redox reactions), as shown in equations 4 and 5.

$$h(t) = mK\left(1 - e^{-\frac{t-\theta}{\tau}}\right) H(t-\theta) \xrightarrow{\theta=0} \quad (4)$$

$$C_{A(0,t)} = M \cdot K \cdot \left(1 - e^{-\frac{t}{\tau}}\right) \quad (5)$$

where M is the concentration of A in the atmosphere and $H(t-\theta)$ is the Heaviside function that can be neglected when the MOS signal is horizontally displaced up to match the delay with the origin of measurement time (i.e., $\theta = 0$).

2.2. Analyte diffusion inside the sensor bulk

Once the vapor has overcome the sensor boundary layer, the analyte A becomes to be consumed by two main processes: surface redox reactions and diffusive process into the bulk due to the porous surface of the sensor. In the case of SnO_2, diffusion into the bulk is usually considered governed by Fick's second law [21,22], see equation 6. The first term on the right is related to the impulse force of bulk diffusion with the Knudsen diffusion coefficient, D_K, [22] and the second one is related to Freundlich adsorption law, simplified by a SnO_2 surface small coverage [10].

$$\frac{\partial C_{A(x,t)}}{\partial t} = D_K\left(\frac{\partial^2 C_{A(x,t)}}{\partial x^2}\right) - \frac{\partial}{\partial t}\left(kC_{A(0,t)}\right) \quad 6$$

where $C_{A(x,t)}$ and $C_{A(0,t)}$ are the concentration of analyte vapor A in depth x (with l as maximum depth) and on surface, respectively. Different analytical solutions for equation 6 are proposed in the literature, depending on the boundary conditions: a) TR, $C_{A(x,0)} = 0$, b) SR, $C_{A(0)} = M$ and $\partial C_{x=l}/\partial x = 0$ being shown in equations 7.1 [23] and 7.2 [21,22], respectively.

$$C_{A(x,t)}^{T.R.} = C_{A(0,t)}\left[1 - erf\left(\frac{x}{2\sqrt{D_K t}}\right)\right] \quad 7.1$$

$$C_{A(x)}^{S.R.} = C_{A(0)} \cdot \frac{\cosh\left[(L-x)\cdot\sqrt{\frac{1}{D_e}}\right]}{\cosh\left[L\cdot\sqrt{\frac{1}{D_e}}\right]}; D_e = \frac{D_K}{1 + R\cdot k} \quad 7.2$$

where D_e is defined as the *efficient diffusion coefficient* to simplify the analytical solution [21]. The depth-concentration profiles can be modelled for TR for an arbitrary D_K showing time dependency, linear profile concentration or SR (i.e., long t values in Fig. 5-a) and diffusion coefficient influence in the concentration profile (Fig. 5-b). Here, R and k the rate constant and the experimental constant of Freundlich from adsorption process, respectively.

[Fig. 5 about here.]

2.3. Influence of the sensor geometry, and the circuitry in signal profile

To determine the relationship between the registered signal and its main features, three additional contributions were deemed necessary: sensor geometry, analyte concentration, and sensor conductance ratio. In equation 8 we present an approximation to consider those variables for Taguchi-type sensors [21].

$$G(t) = \int_0^L \int_0^{2\pi} \int_{R_{ext}-l}^{R_{ext}} H \cdot C_{A(t,0)}\, dr\, d\theta\, dz \qquad 8$$

where L is the sensor length, R_{ext} is the external sensor radius and H the conductance-concentration function. For TR equations 5.2, 7.1, and 8 can be combined to obtain an approximated solution for conductance time dependency, as shown in equation 9.

$$\begin{aligned} G(t) &\cong G_{R_{ext}}(t) \cdot l \cdot \left[erfc\left(\frac{a}{t}\right) - \frac{1}{a\sqrt{\pi}}\left(e^{-\left(\frac{a}{t}\right)^2} - 1\right)\sqrt{t}\right] \xrightarrow{D_k \downarrow\downarrow} G(t) \\ &\cong G_{R_{ext}}(t) \cdot l \cdot erfc\left(\frac{a}{t}\right) \end{aligned} \qquad 9$$

where $G(t)_{T.R.}$ is the conductance approximation for TR, $G_{R_{ext}}$ is the conductance in the sensor external surface, t is the instant considered and a is defined as $l/2\sqrt{D_K}$. In Fig. 6-a is presented the mathematical shape of equation 9 for the first stage of TR where the initial peak is due to the second term of equation, being more relevant when a is abnormally low. In the literature, that situation is named *overshooting* [21,24], and diverse theories have been postulated; however, in this model overshooting is a normal region of MOS response when high diffusive coefficients are considered (i.e., $D_K > 2.5 \cdot 10^{-5} cm^2 \cdot s^{-1}$) or thin sensors. Additionally, Fig. 6-b presents the shape of the equation 9 for our experimental scale of time and realistic values of a from tested vapors. It can be observed the negligible overshooting effect and hence simplification in equation 9 should be an acceptable approximation.

[Fig. 6 about here.]

MOS acquisition circuitry modifies the mathematical expression for data logged (i.e., $G(t) \rightarrow$

$V_{R_L}(t)$), see equation 10.1. Additionally, a linearization that can be observed when low analyte concentration is present [2] (see equation 10.2) because semiconductor current is low.

$$V_{R_L} = V_c \frac{erfc\left(\frac{l}{2t\sqrt{D}}\right) - \frac{2\sqrt{D}}{l\sqrt{\pi}}\left(e^{-\left(\frac{l}{2t\sqrt{D}}\right)^2} - 1\right)\sqrt{t}}{erfc\left(\frac{l}{2t\sqrt{D}}\right) - \frac{2\sqrt{D}}{l\sqrt{\pi}}\left(e^{-\left(\frac{l}{2t\sqrt{D}}\right)^2} - 1\right)\sqrt{t} - \frac{1}{2\pi R_L lL \cdot M\left(1 - e^{-\frac{t-\theta}{\tau}}\right) \cdot H'}} \quad 10.1$$

$$V_{R_L} \cong -2\pi R_L \cdot V_C \cdot L \cdot M \cdot l\left(1 - e^{-\frac{t-\theta}{\tau}}\right) \cdot \left[erfc\left(\frac{l}{2t\sqrt{D}}\right) - \frac{2\sqrt{D}}{l\sqrt{\pi}}\left(e^{-\left(\frac{l}{2t\sqrt{D}}\right)^2} - 1\right)\sqrt{t}\right] H \quad 10.2$$

where $H' = H \cdot K$.

3. Materials and methods

3.1. Analytes

A validation of the theoretical model was implemented with pure substances (i.e., no tagged explosives) listed in Table 1. Those analytes are classified into two main categories: commercial organic solvents and explosives (or close-by chemicals).

Table 1. Vapor pressure of a) organic solvents (ACS grade) [25], and b) explosives (military grade), precursors (pure grade) and closely related chemicals [26–28].

a)

CAS	*IUPAC (common) name*	*Vapor pressure (N.C.)/Pa*
67-56-1	Methanol	$1.3 \cdot 10^4$
64-17-5	Ethanol	$5.9 \cdot 10^3$
115-10-6	Methoxymethane (Dimethyl ether)	$5.9 \cdot 10^4$
67-64-1	Propan-2-one (Acetone)	$2.5 \cdot 10^4$
68-12-2	N,N-dimethylformamide (Dimethylformamide, DMF)	$3.5 \cdot 10^2$
110-54-3	n-Hexane	$1.6 \cdot 10^4$
50-00-0	Formaldehyde (37%)	$5.2 \cdot 10^2$
141-78-6	Ethyl acetate	$9.7 \cdot 10^3$
64-19-7	Acetic acid	$1.5 \cdot 10^3$

b)

CAS	*IUPAC (common) name*	*Vapor pressure (N.C.)/Pa*
100-97-0	1,3,5,7-tetrazatricyclo[3.3.1.13,7]decane (Hexamine)	$4.5 \cdot 10^{-2}$
17088-37-8	3,3,6,6,9,9-hexamethyl-1,2,4,5,7,8-hexaoxonane (Triperoxide Triacetone, TATP) *	6.94
75-52-5	Nitromethane	$3.3 \cdot 10^3$
283-66-9	3,4,8,9,12,13-hexaoxa-1,6-diazabicyclo[4.4.4]tetradecane (Hexamethylene triperoxide diamine, HMTD) *	$33 \cdot 10^{-6}$
121-82-4	1,3,5-trinitroperhydro-1,3,5,triazine (Cyclonite, RDX)	$1.2 \cdot 10^{-7}$
7722-84-1	Hydrogen peroxide	$3.7 \cdot 10^2$

** Synthetized chemicals have GC-MS purity >95%.*

3.2. MOS sensors characterization

Three commercial Taguchi type MOS [19], listed in Table 2, were implemented in the e-nose array. Each sensor possesses a thick sensitive layer of SnO_2 over a cylindrical structure of Al_2O_3 ceramic sustainer, platinum wires and concentric Ni-Cr heater (see Fig. 7-a, b). A microscopic characterization was carried out by a scanning electron microscope, SEM, Hitachi© model S-3400N at 15 kV, including MOS surface doping, observing diverse elements such as praseodymium, aluminum, and sulfur (see Fig. 7-c and Table 2). For micro elemental analysis, an energy dispersive X-ray spectrometer, EDX, Bruker©, Quantax 200 AXD Microanalysis model with XFlash 5010 detector was required.

[Fig. 7 about here.]

Table 2. SEM-EDX characterization of SnO_2 sensors.

Sensor	*Length/* $\boldsymbol{mm}$	$\boldsymbol{\emptyset_{ext}/mm}$	*Sensor thickness/* $\boldsymbol{\mu m}$	*Dopants*	$\boldsymbol{\emptyset_{pore}/\mu m}$
MQ3	4.5 ± 0.3	1.5 ± 0.5	100 ± 50	Pr, Si	~ 7
MQ135	5.0 ± 0.5	1.5 ± 0.5	200 ± 40	Al, Si, Mg, Fe	~ 1
MQ138	5.0 ± 0.5	1.5 ± 0.5	250 ± 50	Al, Si, S	< 0.5

3.3. E-nose architecture and registration circuitry

The e-nose circuitry was designed using PCB Layout© software and manufactured by JLCPCB©, being assembled at our laboratories in a two-device configuration: sensing and recording modules, first one contains an array of sensors and main electronics with a volume of 20 ml where air is forced in a fixed flow rate of 0.5 l/min. The MOS conductance response, G_S, was recorded after voltage conversion, V_{R_L}, by the circuitry shown in Fig. 8, ruled by equation 11

$$\frac{\left(R_L + R_{L\_min}\right) \cdot V_P}{V_{RL}} - R_L = \frac{1}{G_s} \qquad 11$$

where R_L is the load resistance, R_{L_min} is a protective load resistance of circuit, V_P is the polarization voltage (typically 5V), V_{R_L} is the drop voltage of $R_L + R_{L\_min}$ and G_S is the sensor conductance.

An embedded microprocessor governs the main e-nose functions such as sensors operation temperature (i.e., $V_H \cong 4.5 \pm 0.5V$ in Fig. 8) and polarization voltage (i.e., $V_P = 5.0 \pm 0.2\,V$), maintaining a MOS constant temperature around 300^oC. On its part, the second module is responsible for mathematical signal preprocessing and data storage to, finally, data were analyzed offline by MATLAB© developing custom scripts.

[Fig. 8 about here.]

4. Experimental model validation, results, and discussion

Method validation was made by exposing e-noses to different vapor concentration of the analytes listed in Table 1, using Mass Flow Controllers (MFC). The first step was to obtain $\boldsymbol{R}$ data matrix, highlighting relevant information and accentuate model feature extraction. Finally, the application of multivariate algorithms enabled vapor identification.

4.1. Experimental MFC and e-nose setup

A headspace methodology was considered appropriate for vapors generation [3], with a procedure based on dilutions from a saturated atmosphere. Bulk analytes were left enough time in a 5 L closed vessel to reach saturation equilibrium with the surrounding atmosphere. Therefore, a dilution diluted (1:10 maximum) was implemented by a controlled flow of dry air employing two Alicat©, MC-series, schematized in Fig. 9, dragging vapors into the detector chamber in $0.5\ L \cdot min^{-1}$ constant flow for $10\ min$.

[Fig. 9 about here.]

4.2. Data mining: signal preprocessing and model fitting (features extraction)

Commonly manipulation of raw MOS signals, by derivative methods to minimize the quantitative influence in the signal [4,8,13], is not required in presented model, so quantitative information is maintained and extracted afterwards. Additionally, it should have into consideration that sensors chamber design minimizes the free volume between sensors and, their linear disposition of the sensors array in the flow, haven't represented any real-time response influence (see t_a vertical alignment in the three MOS responses before any mathematical manipulation into Fig. 10). Nevertheless, signal preprocessing is required to improve the model's performance: firstly, sensor temporal series were gathered (i.e., $V_{R_L}^{S_n}(t), n \in [1,3]$) to subtract temporal, and voltage, offsets (see Fig. 10-a), minimizing the delay period (i.e., θ) and MOS background (i.e., b_{S_n}). $\boldsymbol{R}$ and $\boldsymbol{t}$ are matrix that gathers the MOS response and timing, respectively. Later, low-pass filter is applied to the higher signal series (i.e., $V_{R_L}^{S_n}(t) < 4.8V\ \forall t$, for TATP, to S_1), high-pass filter thresholds is applied to the lower series (i.e., $V_{R_L}^{S_n}(t) > 1.2V$, for TATP, to S_3) and, finally, a third filter dismiss chemicals below

a prefixed sensitivity threshold (i.e., $\sum V_{R_L}^{S_n}(t) > 7V, \forall t$). All those filters provide shorter matrix (i.e., $\boldsymbol{R_{filt}}, \boldsymbol{t_{filt}}$ see Table 3) reducing the impact of undesirable chemicals. In this process, two relevant instants are determined: t_a and t_b, and signal drift will offer matrix for model fitting: $\boldsymbol{R_{PARC}}$ and $\boldsymbol{t_{PARC}}$.

[Fig. 10 about here.]

Table 3. Data preprocessing rejection rate

Chemical vapor	*Total trials*	*Essays fitted to model*	*Rejecting rate*	*Fitted to the model*
Hexamine	2	0	100%	–
TATP	22	22	0%	√
Nitromethane	6	6	0%	√
HMTD	3	0	100%	–
Methanol	2	0	100%	–
Ethanol	4	3	25%	√
Dimethyl ether	3	0	100%	–
Acetone	9	2	78%	√
DMF	4	0	100%	–
n-Hexane	7	5	14%	√
Formaldehyde	7	5	29%	√
Ethyl acetate	2	0	100%	–
Acetic acid	2	0	100%	–
n	73	43	41%	6

6 chemicals were able to overcome data preprocess for TATP identification, so those are employed for validation in concentrations that are varied 4 orders of magnitude (see Fig. 11), supporting that MOS signals are more influenced by the nature of the analyte than by concentration [2]. In Fig. 12 are shown examples of model good-of-fitness for every chemical where features (see Table 4) are extracted.

[Fig. 11 about here.]

[Fig. 12 about here.]

Table 4. Model features τ and H'

Chemical	*ID*	$\boldsymbol{\tau_{S_1}}$	$\boldsymbol{\tau_{S_2}}$	$\boldsymbol{\tau_{S_3}}$	$\boldsymbol{H'_{S_1}}$	$\boldsymbol{H'_{S_2}}$	$\boldsymbol{H'_{S_3}}$
TATP	1	183	301	279	0.14	0.12	0.05

	2	245	368	313	0.12	0.05	0.21
	3	306	464	334	0.05	0.21	0.18
	4	810	1000	847	0.21	0.18	0.07
	5	446	679	697	0.18	0.07	0.16
	6	679	697	932	0.07	0.16	0.12
	7	697	932	1000	0.16	0.12	0.04
	8	689	1000	597	0.12	0.04	0.17
	9	778	1000	934	0.04	0.17	0.12
	10	1000	1000	668	0.17	0.12	0.05
	11	1000	1000	1000	0.12	0.05	0.15
	12	669	801	640	0.05	0.15	0.12
	13	1000	1000	1000	0.15	0.12	0.06
	14	1000	1000	1000	0.12	0.06	0.16
	15	1000	1000	729	0.06	0.16	0.12
	16	194	629	215	0.16	0.12	0.06
	17	593	508	243	0.12	0.06	0.26
	18	460	896	392	0.06	0.26	0.21
	19	152	187	136	0.26	0.21	0.07
	20	132	286	178	0.21	0.07	0.20
	21	549	1000	263	0.07	0.20	0.15
	22	1000	1000	927	0.2	0.15	0.04
Acetone	23	48.3	56.8	44.7	0.07	0.04	0.03
	24	1000	1000	1000	2.25	2.27	1.21
Hexane	25	57.7	303	1000	0.21	0.51	1.51
	26	16.2	29.2	335	0.26	0.24	1.16
	27	20.96	45.8	205	0.23	0.16	0.41
	28	1000	213	1000	1.47	0.42	2.01
	29	60.2	1000	1000	0.48	3.51	3.24
Formaldehyde	30	88.34	138	144	0.16	0.17	0.09
	31	95.1	143	180	0.17	0.15	0.08
	32	160	220	256	0.16	0.15	0.07
	33	266	290	302	0.14	0.10	0.06
	34	210	242	221	0.12	0.10	0.06
	35	88.34	138	144	0.16	0.17	0.09
Nitromethane	36	77.6	76.3	67.6	0.2	0.21	0.04
	37	84	473	98	0.34	0.97	0.07
	38	123	99.8	57	0.51	0.31	0.07
	39	112	1000	102	0.37	1.77	0.08
	40	48.9	1000	73.8	0.43	2.58	0.09
Ethanol	41	1000	1000	1000	1.80	1.29	0.79
	42	1000	260	218	2.20	0.73	0.25
	43	464	325	99	2.29	1.19	0.17

* τ value is limited to 1000 in fitting process

4.3. Data mining: signal preprocessing and model fitting (features extraction)

Principal Component Analysis (PCA) is a robust linear pattern-recognition technique for e-nose data classification [4,13] when combined with cluster analysis, or other linear tools such as Mahalanobis distance (MD). PCA results are gathered, and scattering visualization is presented in Fig. 13. MD exhibits strong class TATP identification.

[Fig. 13 about here.]

Therefore, 6D MD was calculated, which TATP average value is $\overline{M.d.}_{TATP}^{6DD(p=0.05)} = 2.3 \pm 1.0$.

Table 5. 6D Mahalanobis distances to TATP linear-fitting model

Category	ID	$\boldsymbol{M.d.^{6D}}$	Conc. (g/L)
TATP	1	2.8	4.3E-04
	2	2.1	4.9E-04
	3	2.3	3.6E-04
	4	2.4	2.1E-04
	5	2.2	2.9E-04
	6	2.4	1.8E-04
	7	2.2	4.0E-04
	8	2.4	2.4E-04
	9	2.0	2.7E-04
	10	2.5	3.4E-04
	11	1.8	3.2E-04
	12	1.6	1.8E-04
	13	1.5	2.7E-04
	14	1.8	1.1E-04
	15	2.1	3.2E-04
	16	2.9	5.9E-04
	17	3.0	5.6E-04
	18	3.2	4.9E-04
	19	3.3	6.0E-04
	20	2.4	6.0E-04
	21	2.7	5.4E-04
	22	2.1	3.2E-04
Acetone	23	6.1	1.8E-01
	24	91.6	6.0E-01
Hexane	25	36.8	4.4E-01
	26	24.9	4.5E-01
	27	7.5	4.7E-01
	28	65.9	4.8E-01
	29	121.1	5.6E-01
Formaldehyde	30	2.6	6.4E-03
	31	2.6	6.4E-03
	32	2.5	6.2E-03

	33	2.9	6.0E-03
	34	3.4	4.9E-03
	35	3.5	6.9E-02
Nitromethane	36	17.5	7.7E-02
	37	8.8	8.0E-02
	38	33.4	7.7E-02
	39	49.9	8.0E-02
	40	61.1	9.1E-02
Ethanol	41	51.8	9.4E-02
	42	58.1	1.1E-01
	43	2.8	4.3E-04

It can be observed that a swift TATP identification can be achieved with a positive identification of the 100% TATP trials, dismissing the rest of chemicals except formaldehyde, that presents a high rate of false positives (i.e., ~60%), being indistinguishable from highly concentrated TATP (see Fig. 14).

[Fig. 14 about here.]

5. Conclusions and outlook

This manuscript presents a methodology to reach a successful chemical vapor identification for TATP, a concerning HME, by an e-nose witch response is based on an array of three MOS sensors. Along the document data preprocess methodology is described without any normalization stage (e.g., derivative) allowing to retain the quantitative information which other methods dismiss because same Transitory Region, depending on is considered at beginning or at the end was identified as a different vapor. By contrast, proposed model covers all range of concentrations, naturally emitted by TATP (e.g., no heating) and all regions of Transitory Region of signals (i.e., from 1τ to 4τ) fitted by same model with the same features, remaining qualitative and quantitative information.

For those purposes, a response model for MOS sensors was theoretically deduced and, as an additional hit of the model, some signal abnormalities reported in bibliography, such as overshooting effect, can be easily explained by this response model. Later, manuscript describe in detail two model features (i.e., H and τ), besides feature extraction methodology and experimental methodology validation versus 6 chemical vapors. Finally, analysis of features combining Principal Component Analysis and Mahalanobis distance, demonstrated a real-time, and successful, process to identify TATP in full range of vapor concentrations naturally emitted by solid explosive

Results have shown a linearization for those features versus vapor concentration, despite the obvious non-linear MOS response nature. That result seems to be a powerful tool for explosive identification because zooming out the e-nose, in case of doubt, should give the same identification. Unfortunately, array simplicity, designed for portable enoses, seems to be, at least, partially responsible for a formaldehyde high rate of false positives, intermingling data with highly concentrated TATP. Nevertheless, the presented model and methodology should be considered a relevant step for implementing e-noses in security devices where continuous screening is required.

6. Funding

This research was funded by INTA internal project “ENASUS” (S.IGD21001) and by University of Valladolid under PhD Program.

Acknowledgements

The authors want to thanks to *Instituto de Técnica Aeroespacial* (INTA), from Spanish Ministry of Defense, for the access to energetic materials and technical resources.

References

[1] W. Zhang, Y. Tang, A. Shi, L. Bao, Y. Shen, R. Shen, Y. Ye, Recent Developments in Spectroscopic Techniques for the Detection of Explosives, Materials. 11 (2018) 1364. https://doi.org/10.3390/ma11081364.

[2] G. Xie, X. Lv, P. Zhang, B. Liu, L. Gao, J. Duan, B. Ma, Z. Wu, Uncontactless detection of improvised explosives TATP realized by Au NCs tailored PPV flexible photoelectric Schottky sensor, Nano Select. 1 (2020) 419–431. https://doi.org/10.1002/nano.202000044.

[3] L.E. DeGreeff, K.J. Johnson, Considerations in the vapor analysis of traditional vs. homemade explosives, in: 2017 ISOCS/IEEE International Symposium on Olfaction and Electronic Nose (ISOEN), IEEE, 2017: pp. 1–3. https://doi.org/10.1109/ISOEN.2017.7968849.

[4] A.N. Yumang, A.C. Paglinawan, J.S. Andres, R.J. De Leon, J.C. Dela Cruz, C.K. Floresta, Electronic Nose for detecting Acetone as a Potential Precursor in Triacetone Triperoxide (TATP)-based Improvised Explosive Devices (IEDs), in: Proceedings of the 2020 12th International Conference on Computer and Automation Engineering, ACM, New York, NY, USA, 2020: pp. 52–55. https://doi.org/10.1145/3384613.3384625.

[5] K. Furton, The scientific foundation and efficacy of the use of canines as chemical detectors for explosives, Talanta. 54 (2001) 487–500. https://doi.org/10.1016/S0039-9140(00)00546-4.

[6] M.A. Mäkinen, O.A. Anttalainen, M.E.T. Sillanpää, Ion Mobility Spectrometry and Its Applications in Detection of Chemical Warfare Agents, Anal Chem. 82 (2010) 9594–9600. https://doi.org/10.1021/ac100931n.

[7] T. Wasilewski, J. Gębicki, Emerging strategies for enhancing detection of explosives by artificial olfaction, Microchemical Journal. 164 (2021) 106025. https://doi.org/10.1016/j.microc.2021.106025.

[8] J.W. Gardner, J. Yinon, eds., Electronic Noses & Sensors for the Detection of Explosives, Springer Netherlands, Dordrecht, 2004. https://doi.org/10.1007/1-4020-2319-7.

[9] R. Matyáš, J. Šelešovský, Power of TATP based explosives, J Hazard Mater. 165 (2009) 95–99. https://doi.org/10.1016/j.jhazmat.2008.09.063.

[10] J.W. Gardner, P.N. Bartlett, A brief history of electronic noses, Sens Actuators B Chem. 18 (1994) 210–211. https://doi.org/10.1016/0925-4005(94)87085-3.

[11] D.J. Klapec, G. Czarnopys, J. Pannuto, Interpol review of detection and characterization of explosives and explosives residues 2016-2019, Forensic Sci Int. 2 (2020) 670–700. https://doi.org/10.1016/j.fsisyn.2020.01.020.

[12] M.J. Pavlovich, B. Musselman, A.B. Hall, Direct analysis in real time-Mass spectrometry (DART-MS) in forensic and security applications, Mass Spectrom Rev. 37 (2018) 171–187. https://doi.org/10.1002/mas.21509.

[13] J.W. Gardner, Detection of vapours and odours from a multisensor array using pattern recognition Part 1. Principal component and cluster analysis, Sens Actuators B Chem. 4 (1991) 109–115. https://doi.org/10.1016/0925-4005(91)80185-M.

[14] Z. Hua, C. Tian, D. Huang, W. Yuan, C. Zhang, X. Tian, M. Wang, E. Li, Power-law response of metal oxide semiconductor gas sensors to oxygen in presence of reducing gases, Sens Actuators B Chem. 267 (2018) 510–518. https://doi.org/10.1016/j.snb.2018.04.002.

[15] N. Barsan, U. Weimar, Conduction Model of Metal Oxide Gas Sensors, J Electroceram. 7 (2001) 143–167. https://doi.org/10.1023/A:1014405811371.

[16] G. Korotcenkov, Metal oxides for solid-state gas sensors: What determines our choice?, Materials Science and Engineering: B. 139 (2007) 1–23. https://doi.org/10.1016/j.mseb.2007.01.044.
[17] A. Chaiyboun, R. Traute, T. Haas, O. Kiesewetter, T. Doll, A logarithmic multi-parameter model using gas sensor main and cross sensitivities to estimate gas concentrations in a gas mixture for SnO2 gas sensors, Sens Actuators B Chem. 123 (2007) 1064–1070. https://doi.org/10.1016/j.snb.2006.11.012.
[18] S. Hirobayashi, Dynamic model to estimate the dependence of gas sensor characteristics on temperature and humidity in environment, Sens Actuators B Chem. 60 (1999) 78–82. https://doi.org/10.1016/S0925-4005(99)00249-X.
[19] P.K. Clifford, D.T. Tuma, Characteristics of semiconductor gas sensors II. transient response to temperature change, Sensors and Actuators. 3 (1982) 255–281. https://doi.org/10.1016/0250-6874(82)80027-9.
[20] S. Strässler, A. Reis, Simple models for N-type metal oxide gas sensors, Sensors and Actuators. 4 (1983) 465–472. https://doi.org/10.1016/0250-6874(83)85058-6.
[21] H. Lu, W. Ma, J. Gao, J. Li, Diffusion-reaction theory for conductance response in metal oxide gas sensing thin films, Sens Actuators B Chem. 66 (2000) 228–231. https://doi.org/10.1016/S0925-4005(00)00370-1.
[22] G. Sakai, N. Matsunaga, K. Shimanoe, N. Yamazoe, Theory of gas-diffusion controlled sensitivity for thin film semiconductor gas sensor, Sens Actuators B Chem. 80 (2001) 125–131. https://doi.org/10.1016/S0925-4005(01)00890-5.
[23] G.N. ADVANI, P. KLUGE-WEISS, R.L. LONGINI, A.G. JORDAN, Oxygen vacancy diffusion in SnO_2 thin films, International Journal of Electronics. 48 (1980) 403–411. https://doi.org/10.1080/00207218008901117.
[24] P.D. Skafidas, D.S. Vlachos, J.N. Avaritsiotis, Modelling and simulation of abnormal behaviour of thick-film tin oxide gas sensors in CO, Sens Actuators B Chem. 21 (1994) 109–121. https://doi.org/10.1016/0925-4005(94)80012-X.
[25] J.A. Dean, ed., Lange's Handbook of Chemistry, 15th Edition, McGraw-Hill, INC. , 1999.
[26] J. Oxley, J. Smith, K. Shinde, J. Moran, Determination of the Vapor Density of Triacetone Triperoxide (TATP) Using a Gas Chromatography Headspace Technique, Propellants, Explosives, Pyrotechnics. 30 (2005) 127–130. https://doi.org/10.1002/prep.200400094.
[27] M.J. Aernecke, T. Mendum, G. Geurtsen, A. Ostrinskaya, R.R. Kunz, Vapor Pressure of Hexamethylene Triperoxide Diamine (HMTD) Estimated Using Secondary Electrospray Ionization Mass Spectrometry, J Phys Chem A. 119 (2015) 11514–11522. https://doi.org/10.1021/acs.jpca.5b08929.
[28] T.R. Gibbs, A. Popolato, eds., LASL explosive property data, Univ. California Press, 1980.

Figures

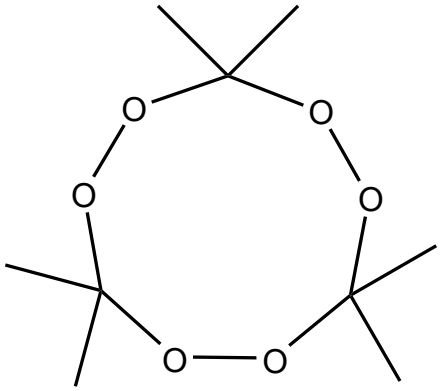

Fig. 1- Triacetone triperoxide (TATP)

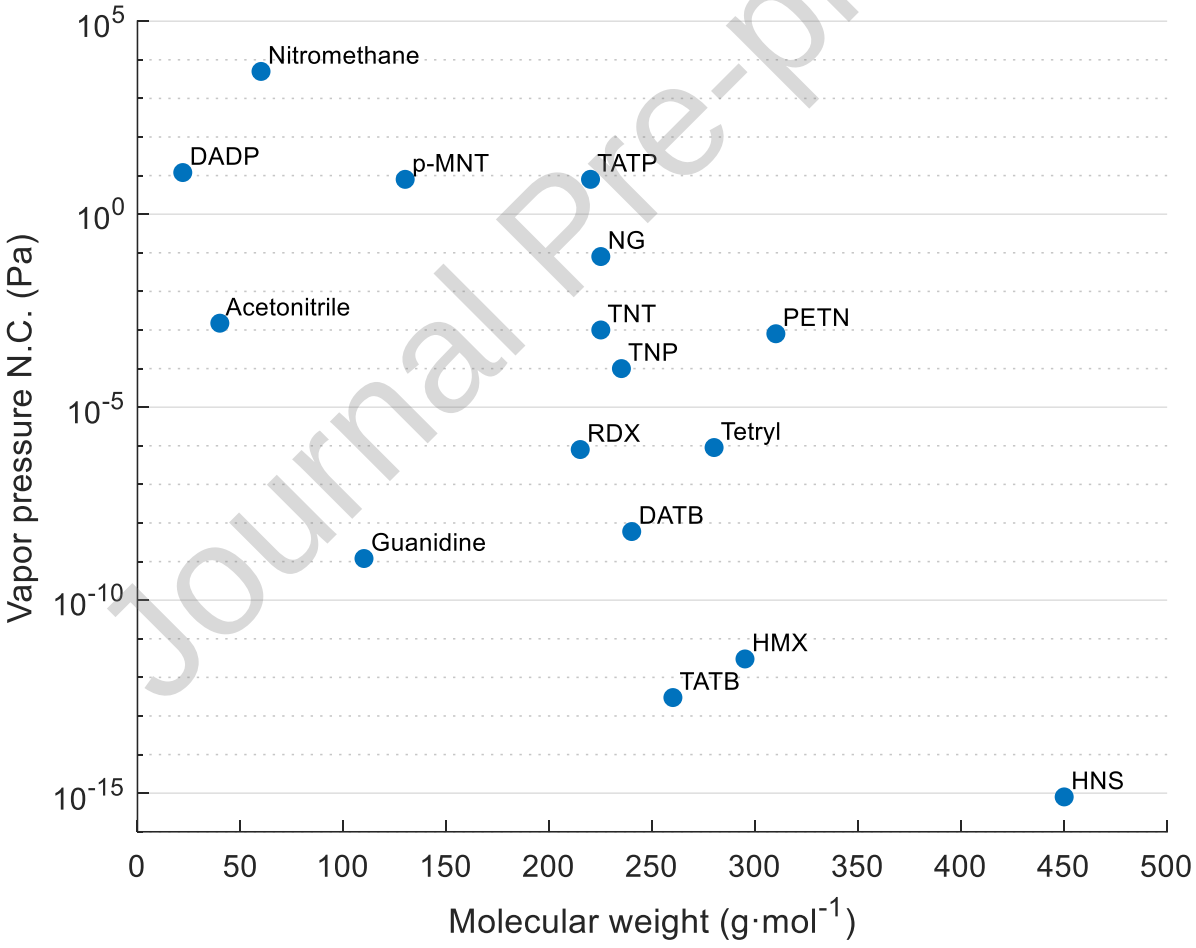

Fig. 2- Vapor pressure of some explosives and close-by chemicals in normal condition (N.C.) adapted from [8,9]

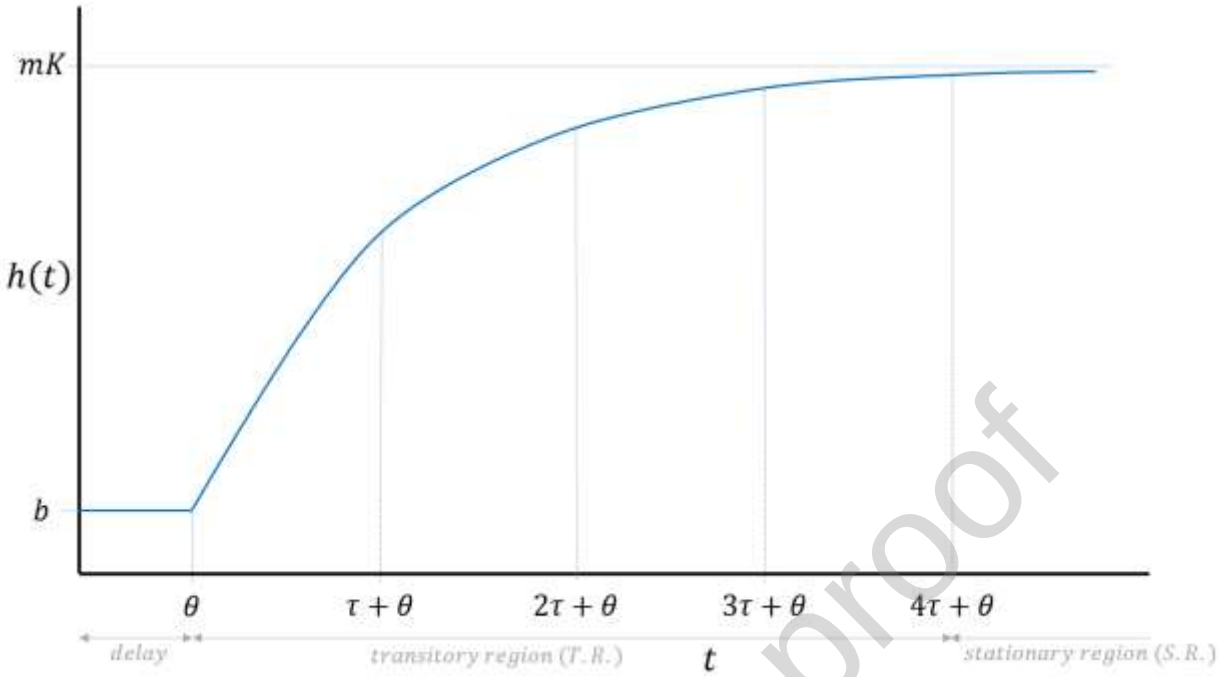

Fig. 3- Scheme of RC model showing some of the main model features

a)

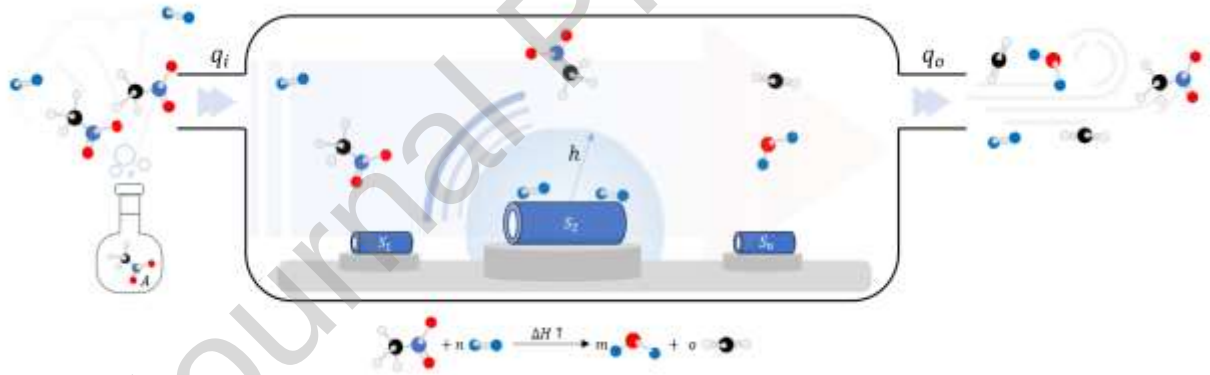

b)

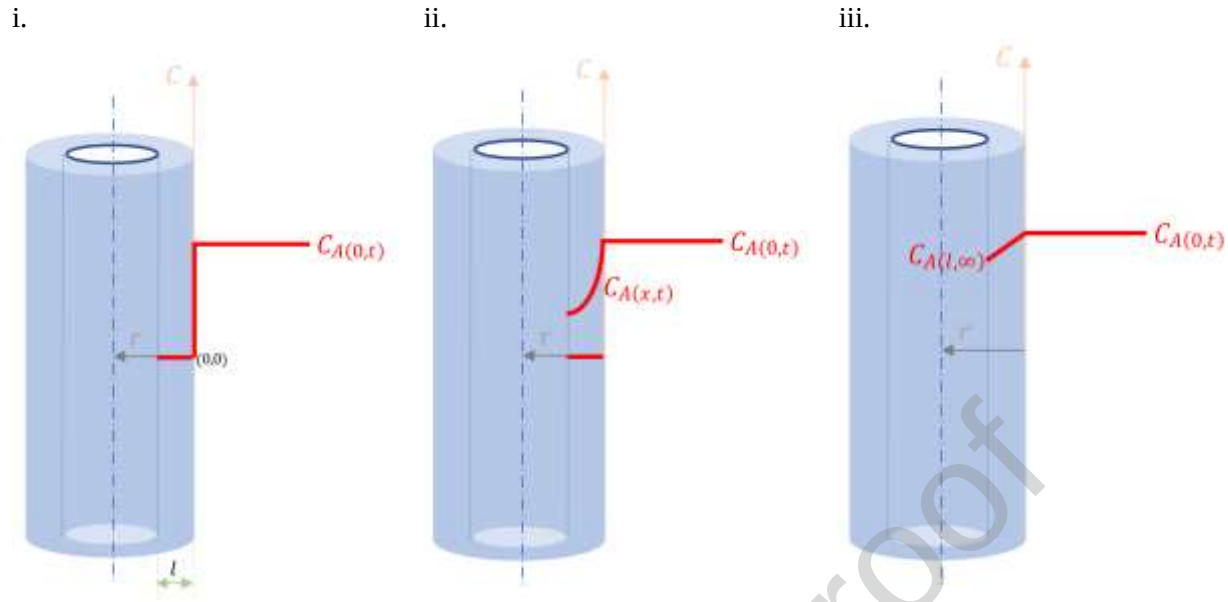

Fig. 4- Vapor diffusion stages in a cylindrical MOS from a) atmosphere to sensor surface, b) sensor surface to bulk in different stages (i. $t = 0$, ii. $T.R.$, iii. $S.R.$)

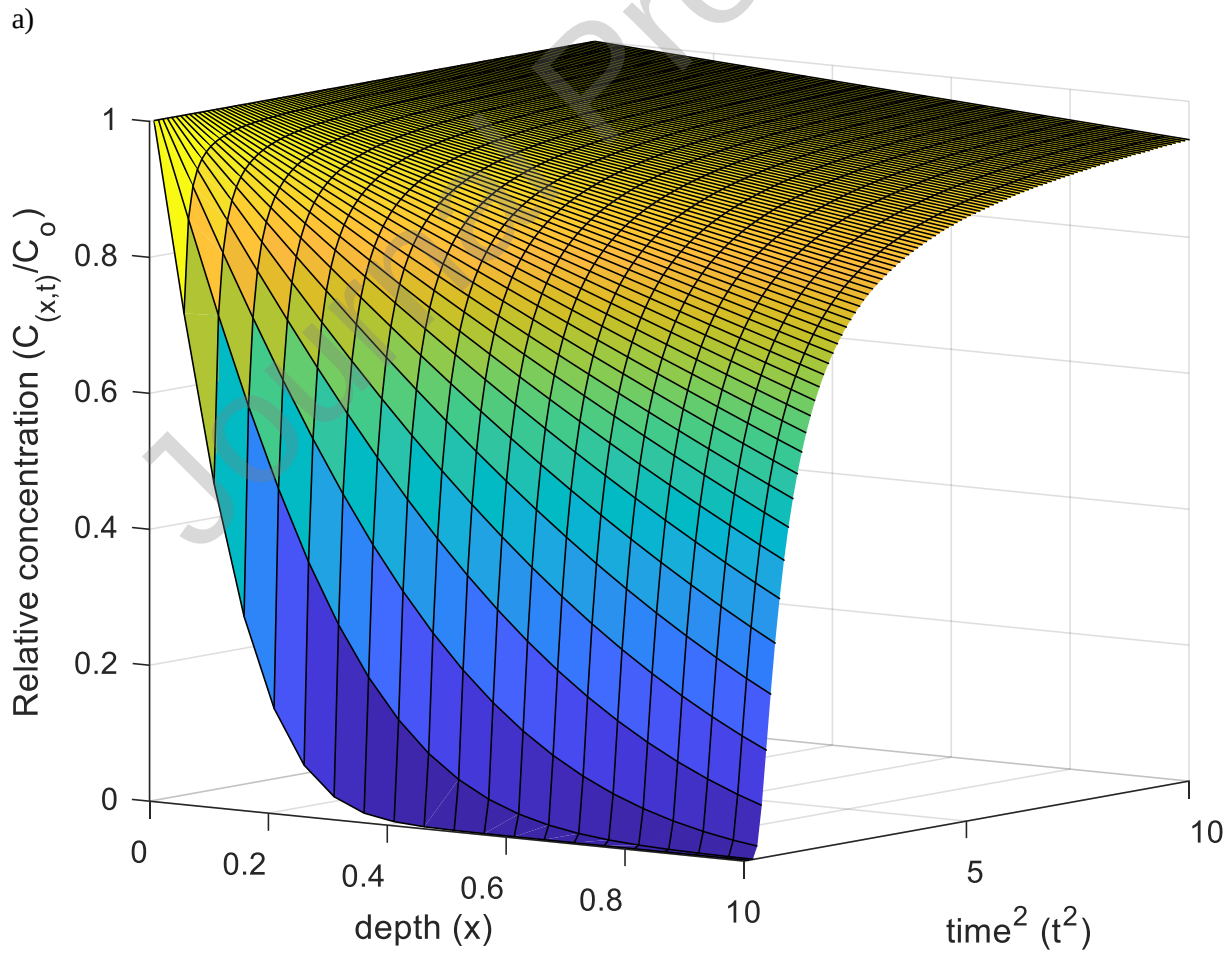

b)

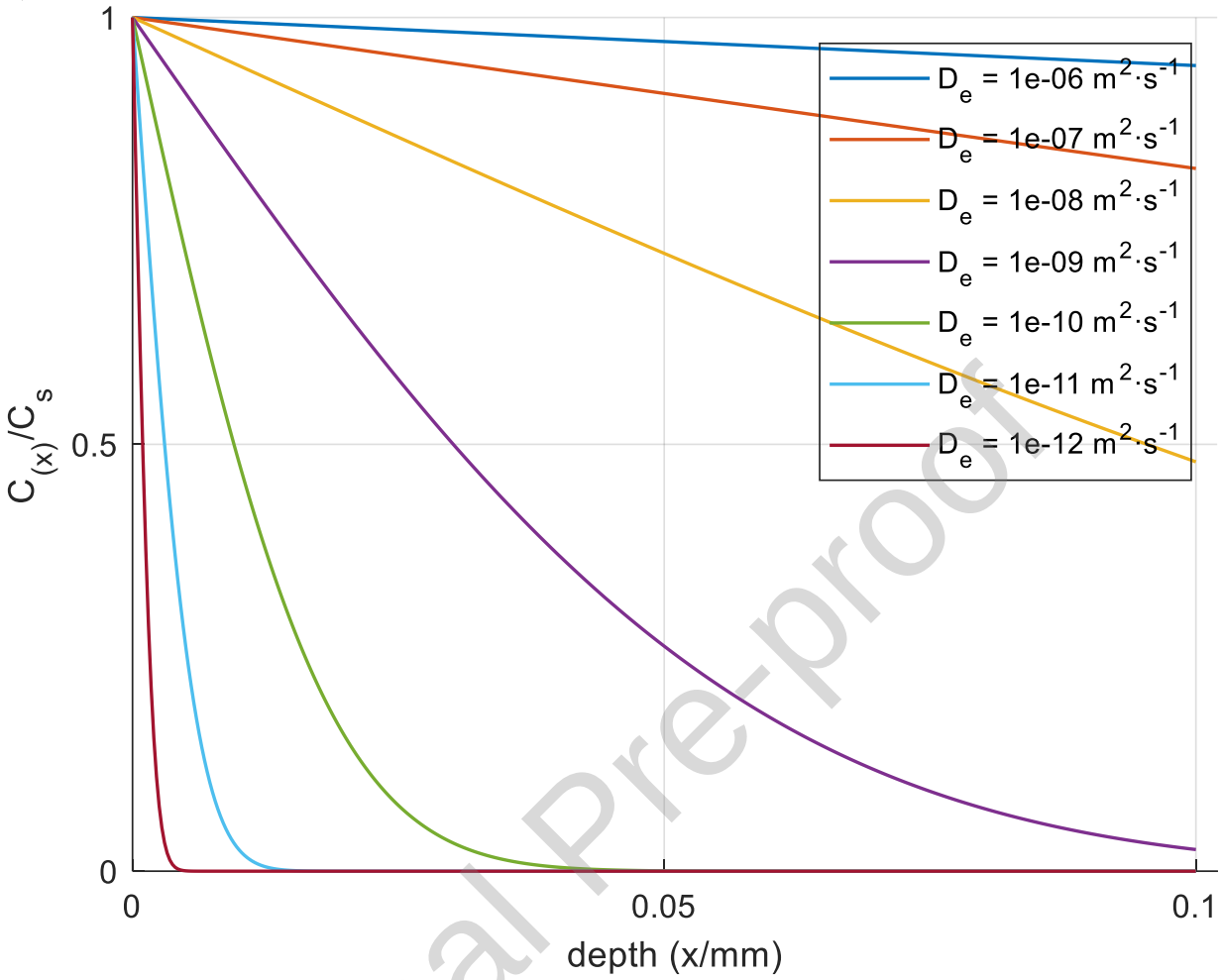

Fig. 5- Relative concentration profile, $1 - erf\left(\frac{x}{2\sqrt{t}}\right)$, in MOS for transitory regions a) temporal evolution and b) diffusion coefficient influence.

a)

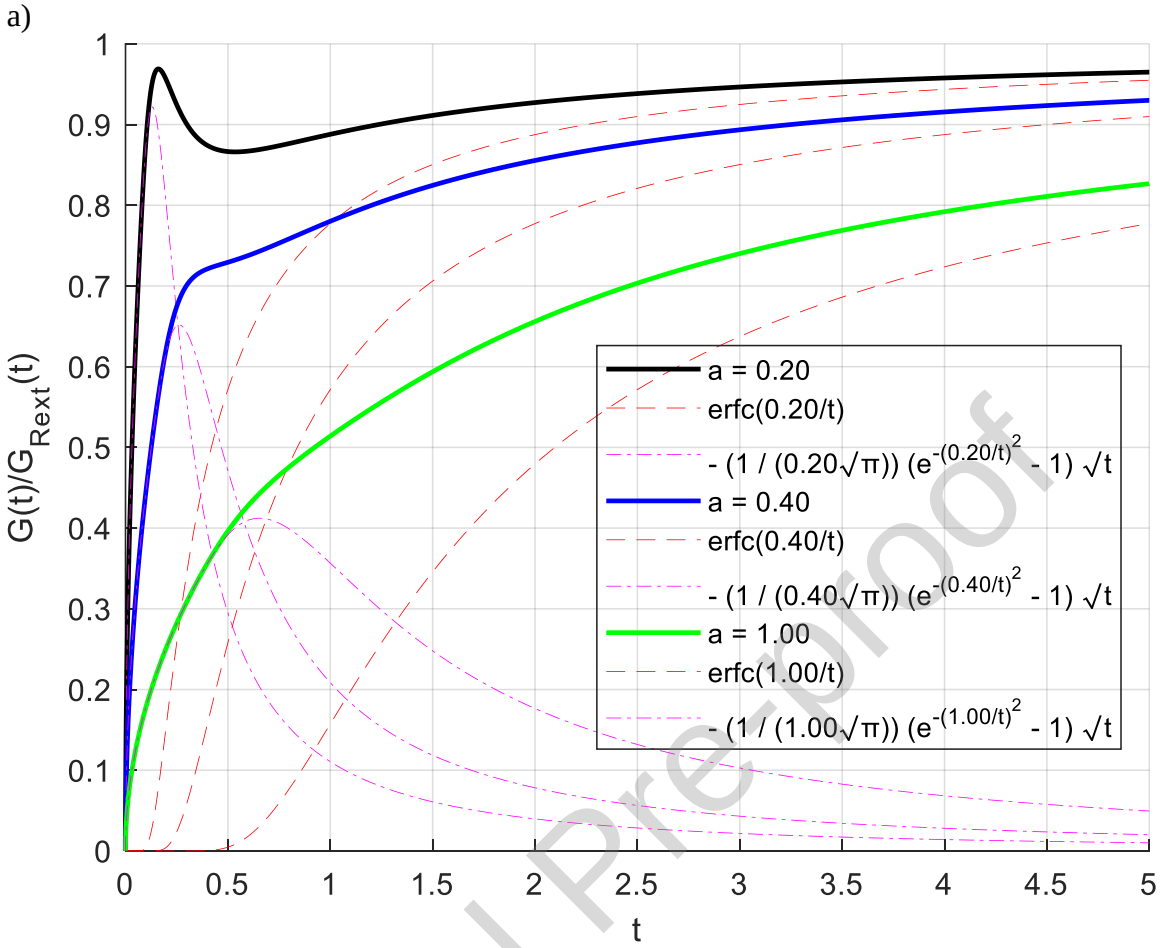

b)

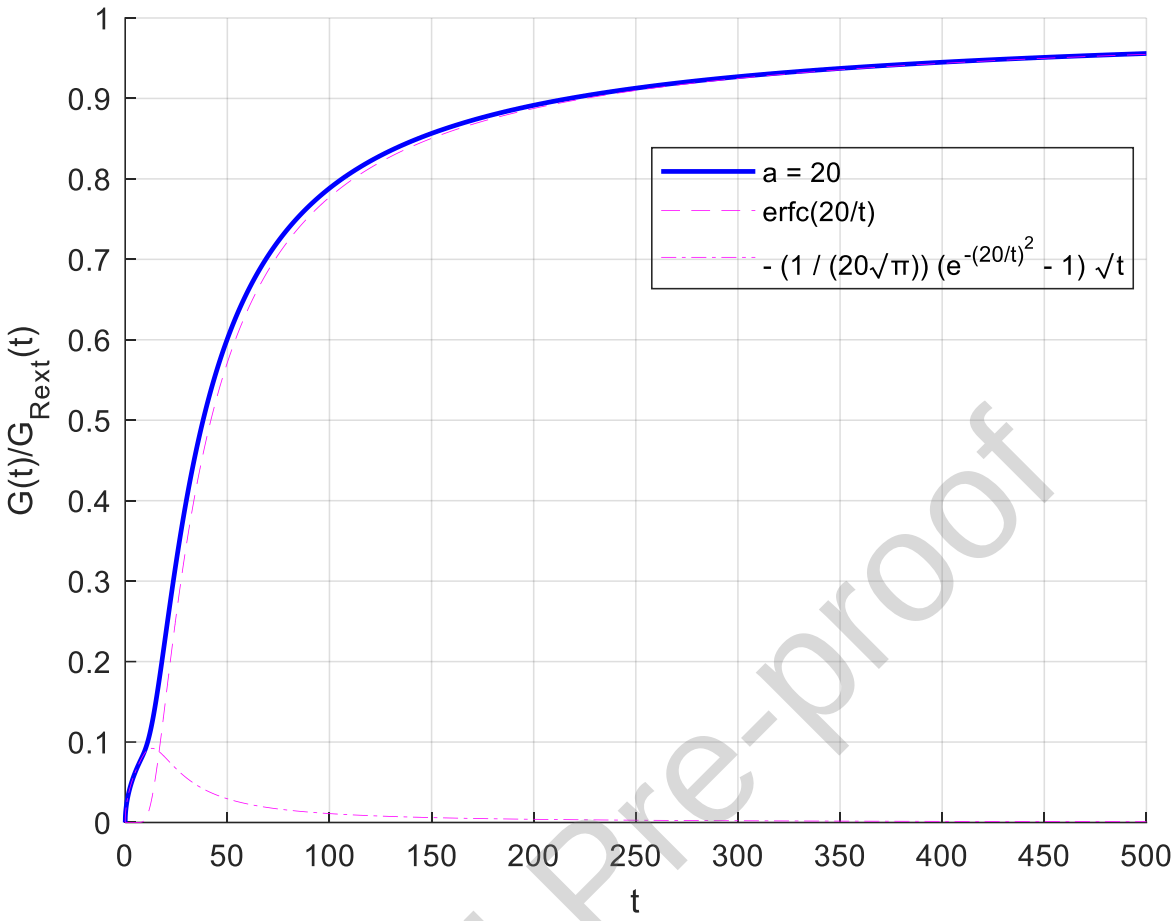

Fig. 6- Shape of $G(a,t)_{T.R.}/G_{R_{ext}}$ ($l = 1\,mm$), for a) D_K ↑↑, overshooting is observed, b) $D_K = 2.5 \cdot 10^{-5}\ cm^2 \cdot s^{-1}$ in normal time scale no overshooting is observed.

a)

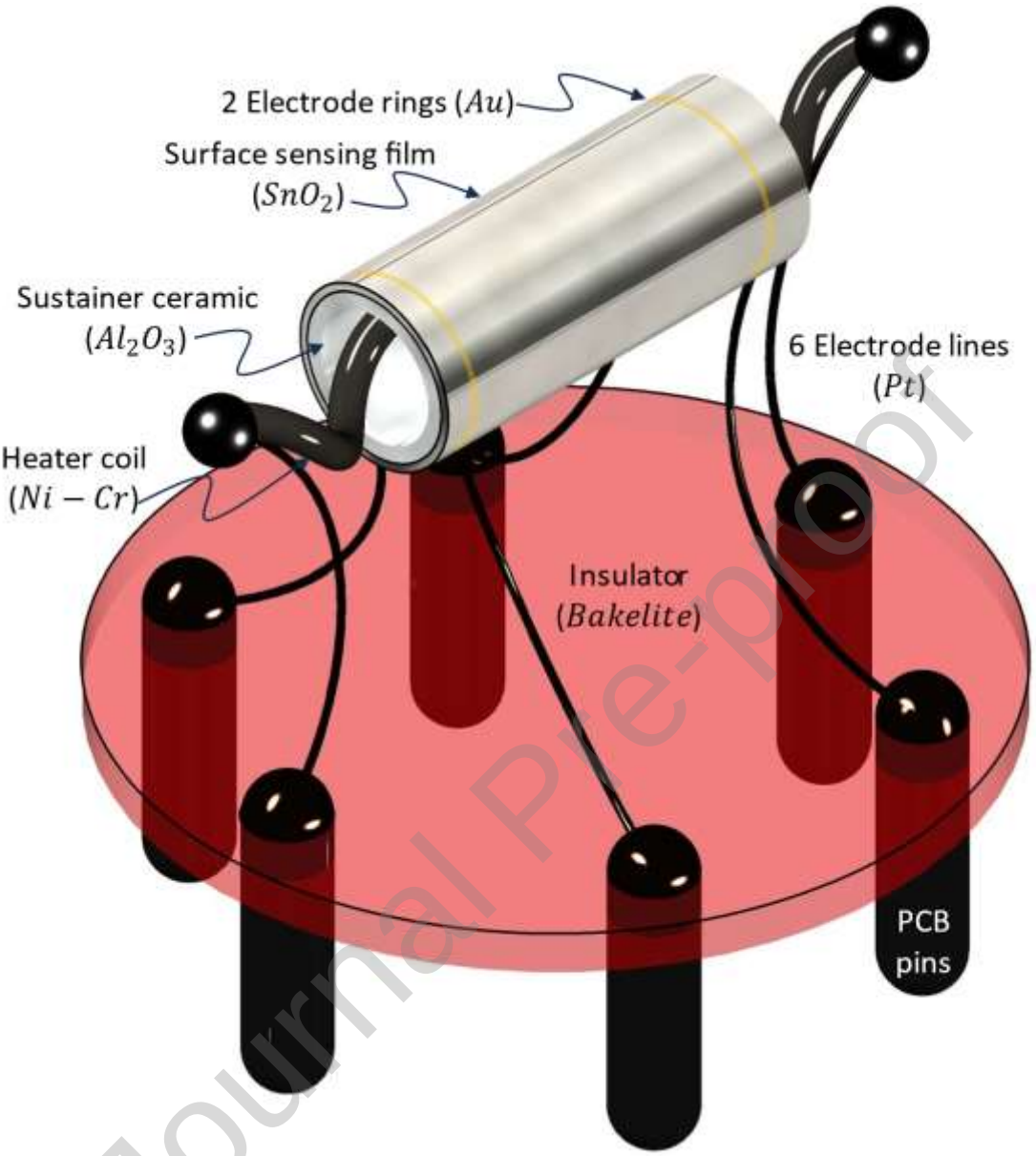

b)

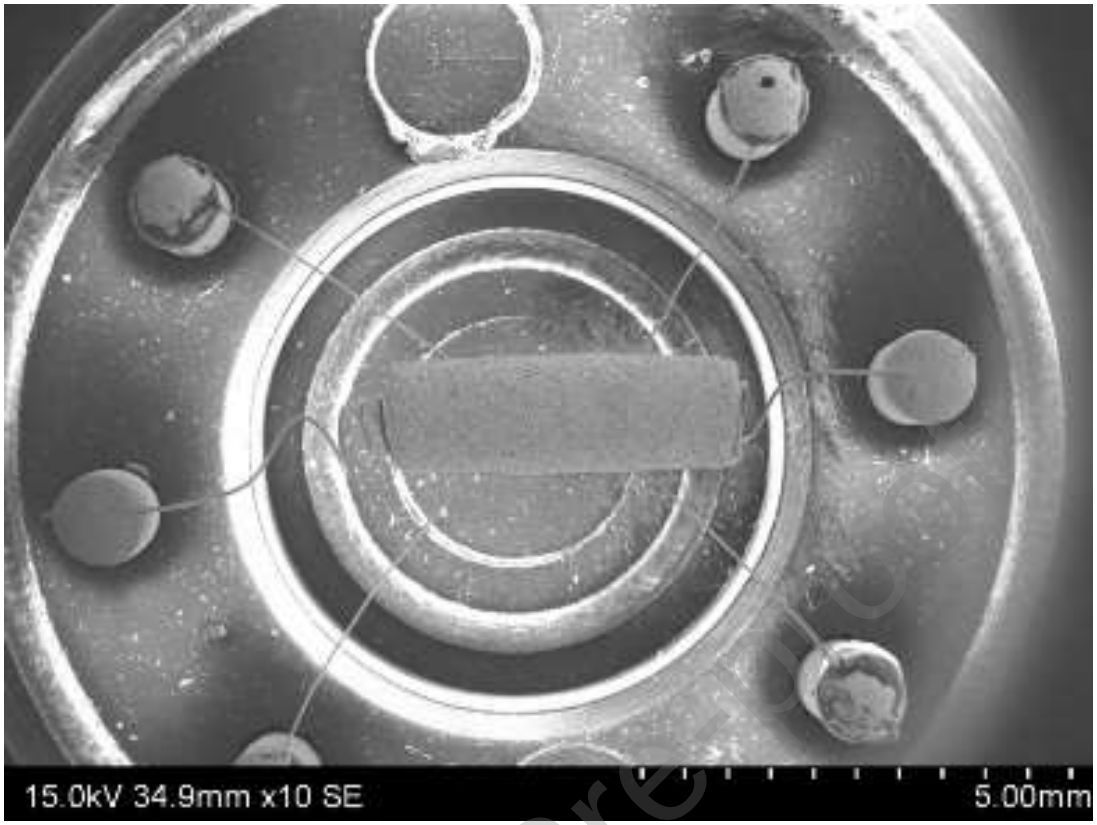

c)

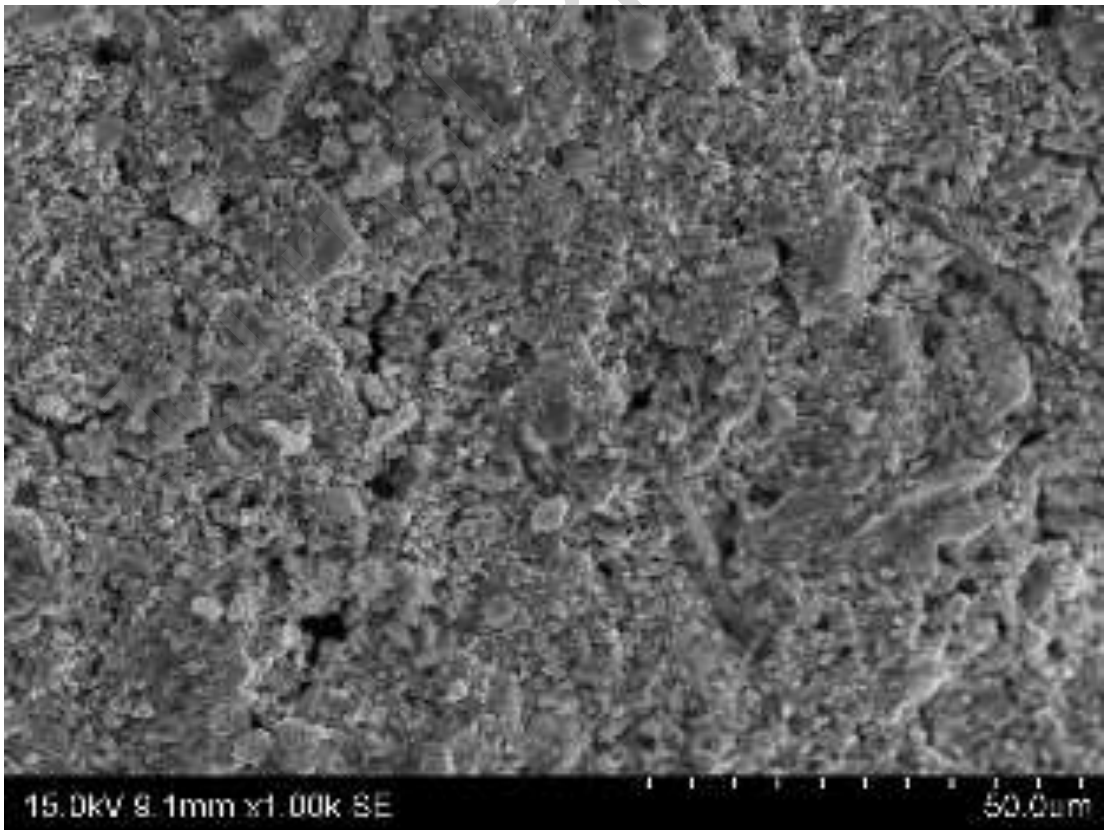

Fig. 7- MOS Taguchi sensors a) scheme, b) SEM sensor overview, c) porous surface (SEM).

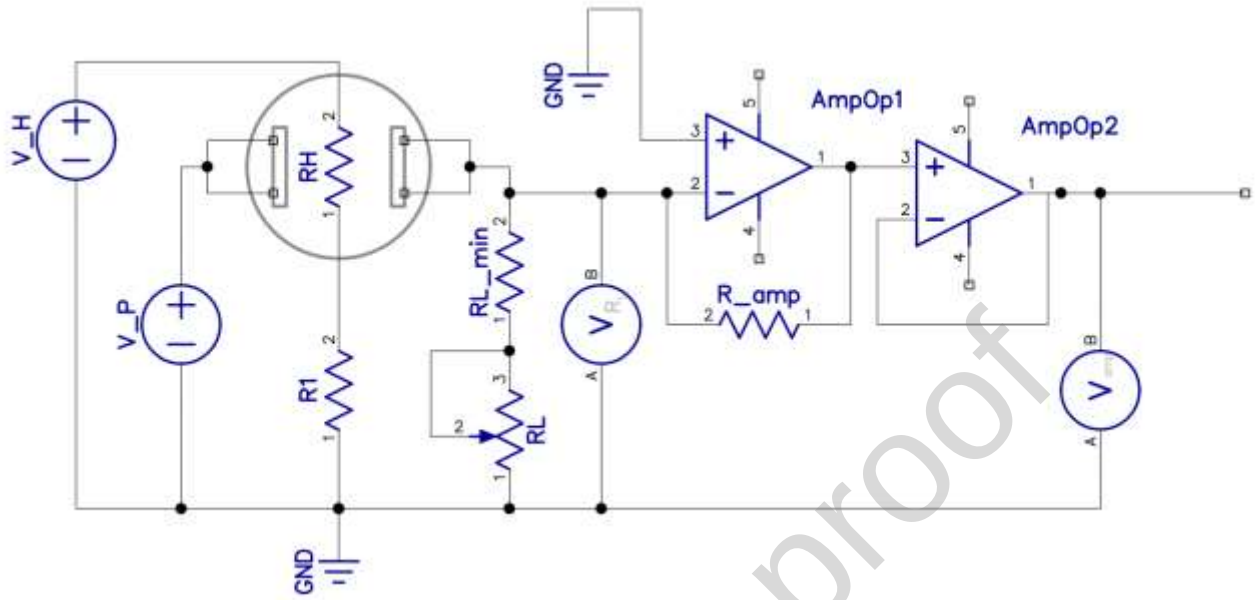

Fig. 8- Acquisition circuitry by voltage divider

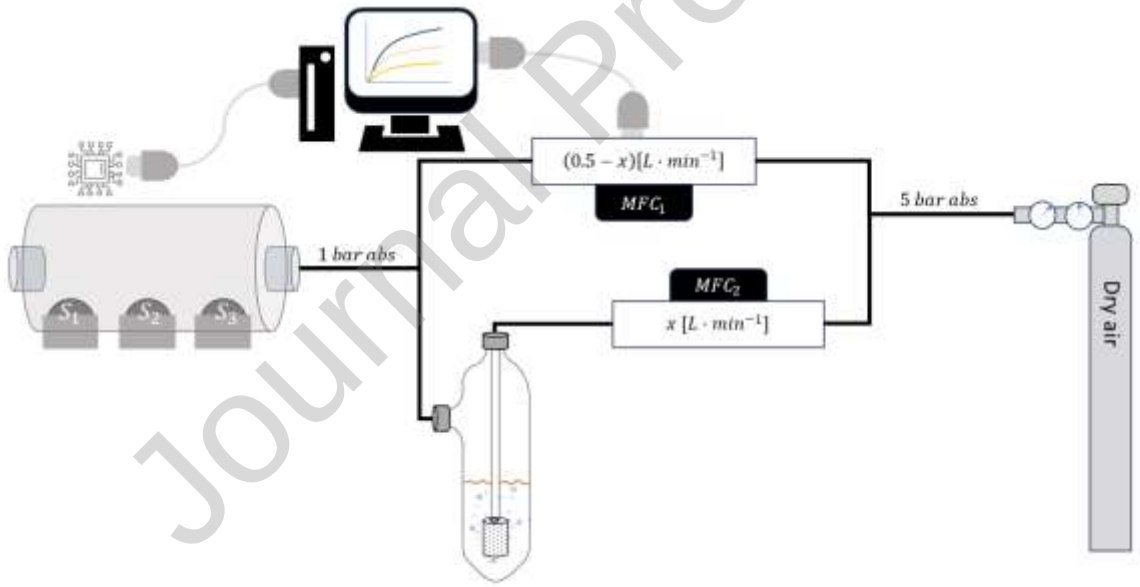

Fig. 9- Scheme of methodology and main elements with bubbler and MFC

a)

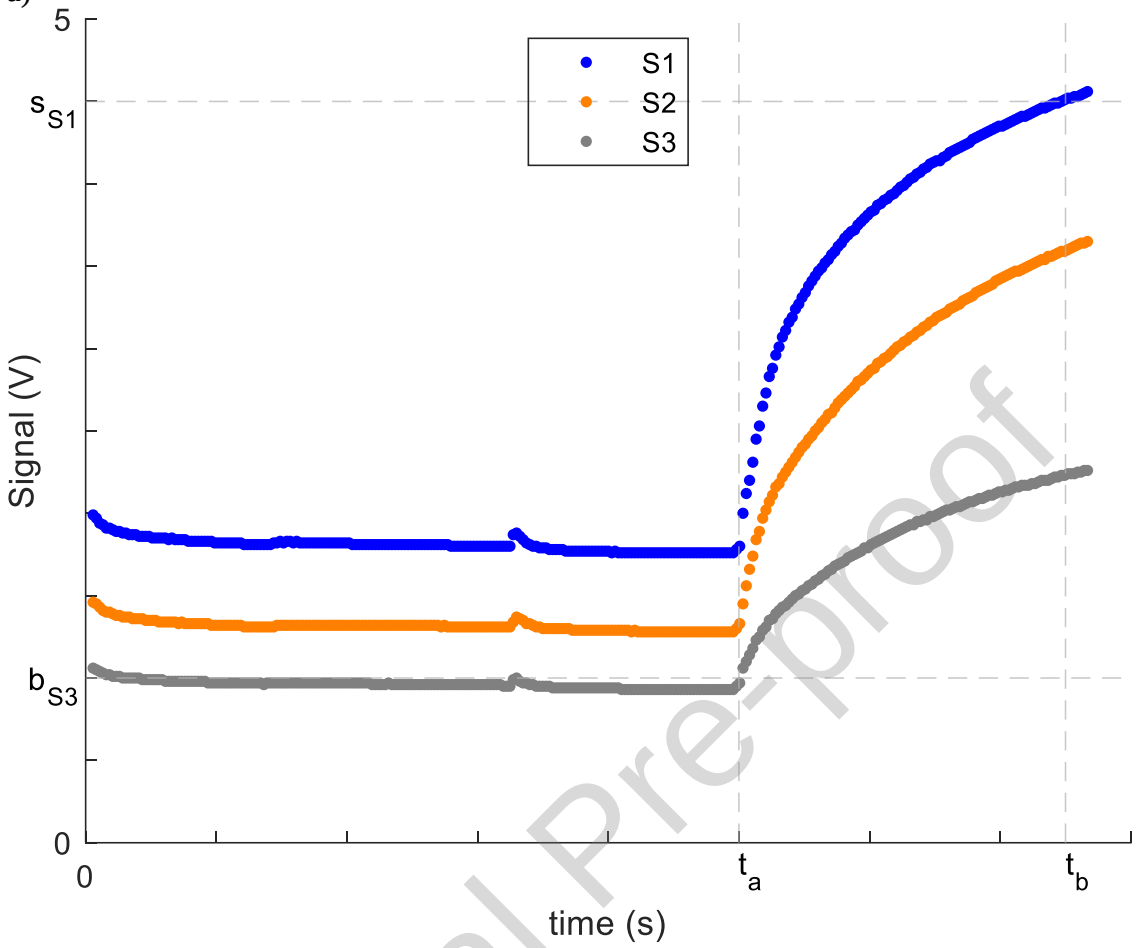

b)

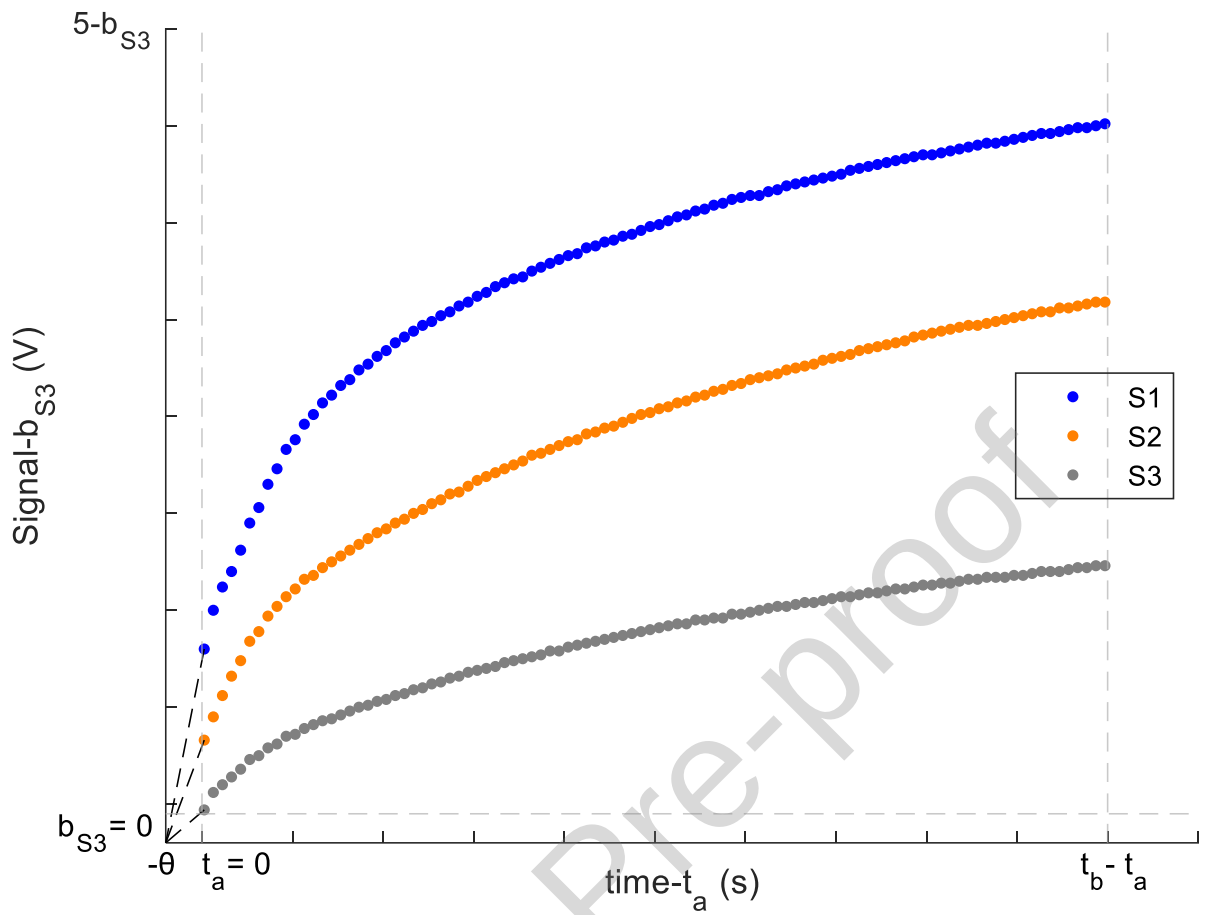

Fig. 10- Data mining, a) e-nose full signal record (i.e., $\boldsymbol{R}$ vs $\boldsymbol{t}$), b) preprocessing signal trim and shift (i.e., $\boldsymbol{R_{PARC}}$ vs $\boldsymbol{t_{PARC}}$) features extraction in R-C model

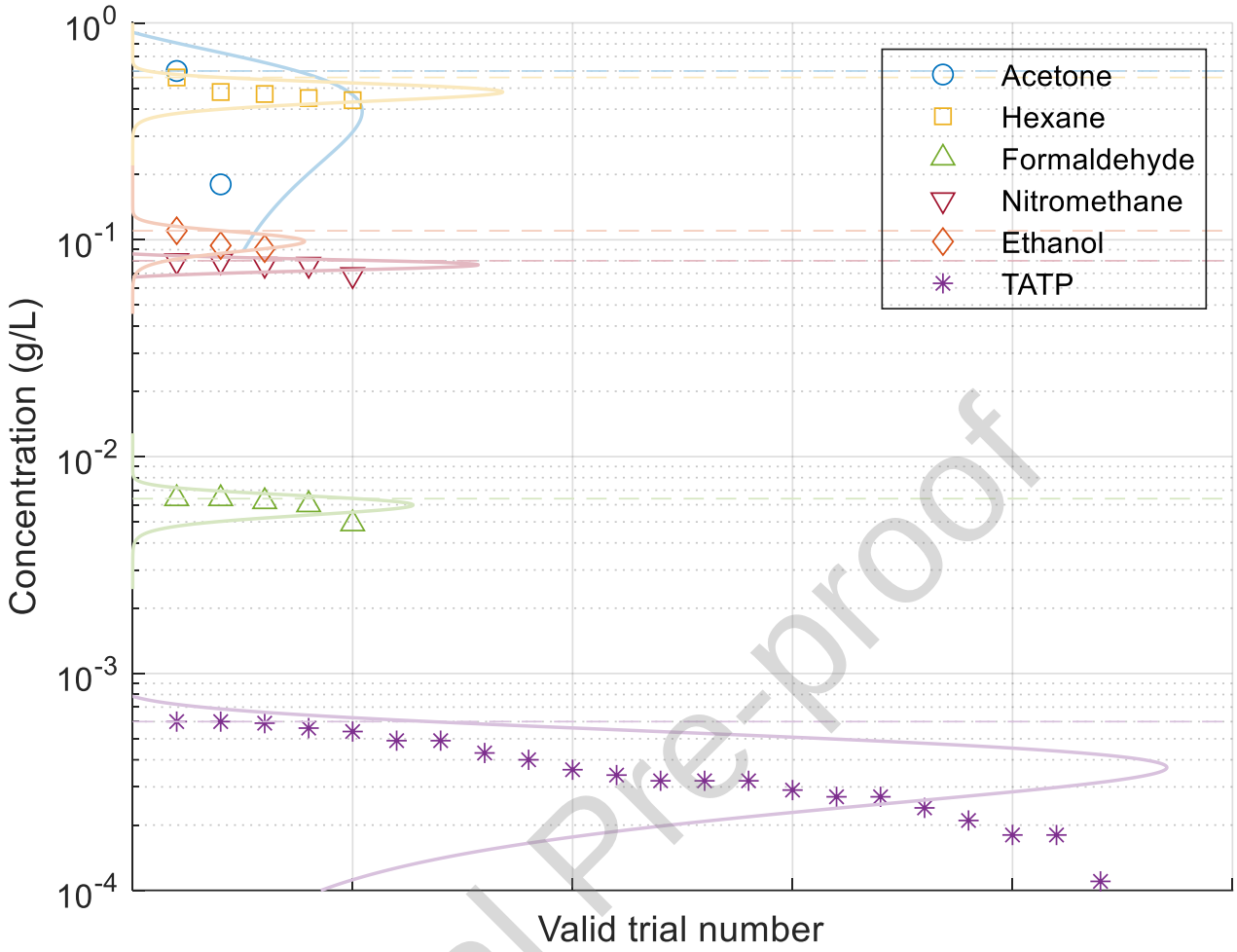

Fig. 11- Concentration in air of each valid trial obtained by dilution from saturated state in N.C. (dotted line) and gaussian estimated distribution.

a)

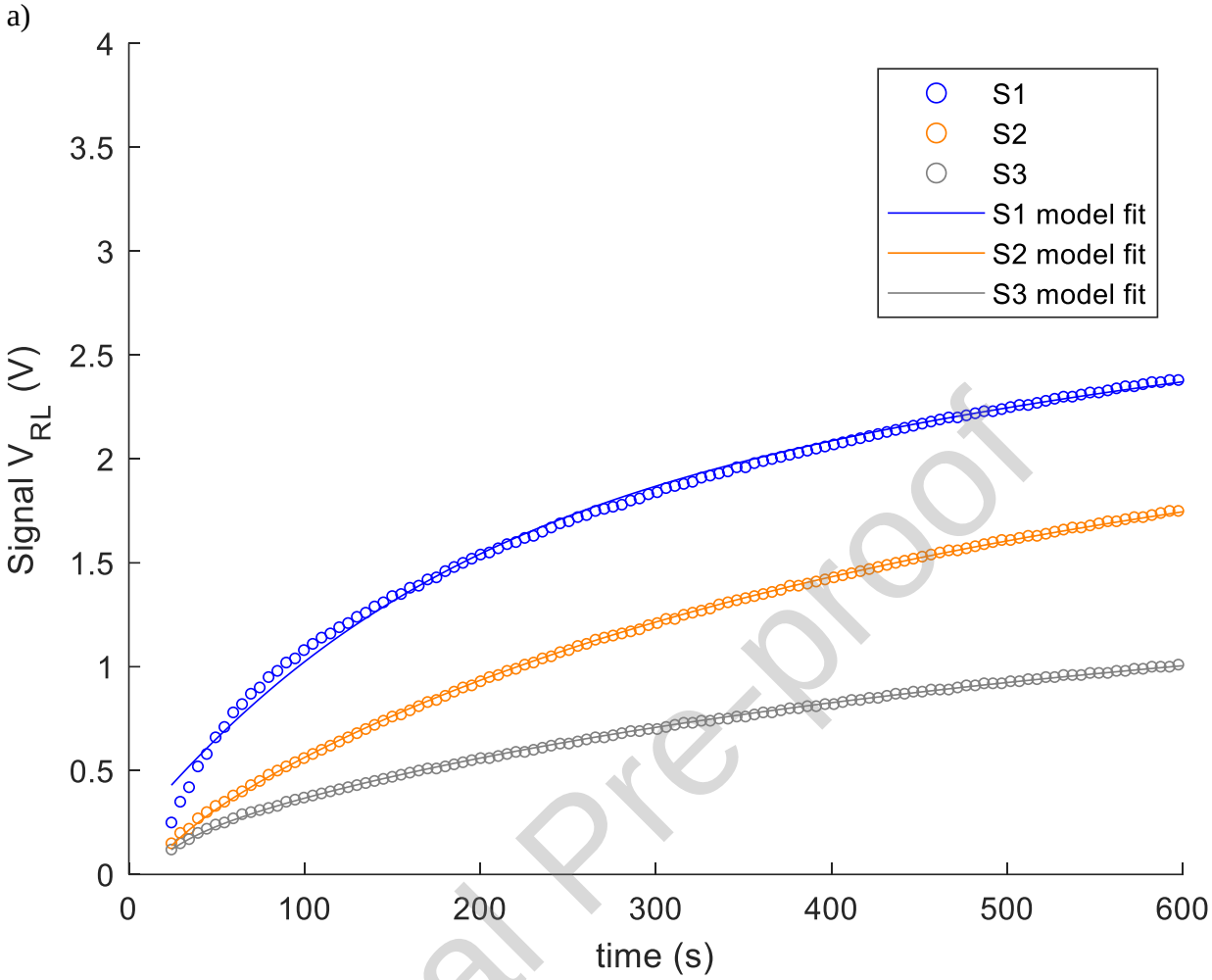

b)

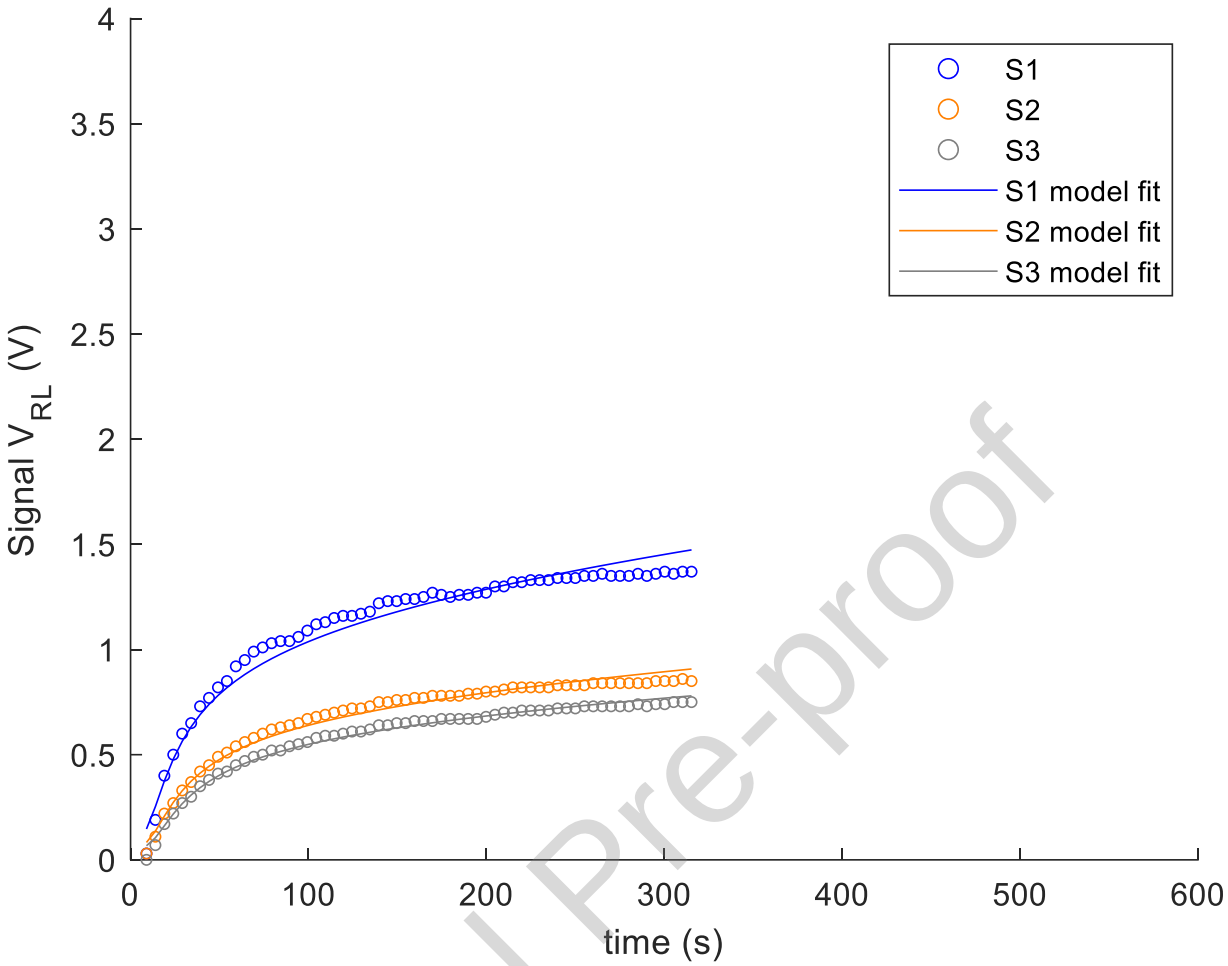

c)

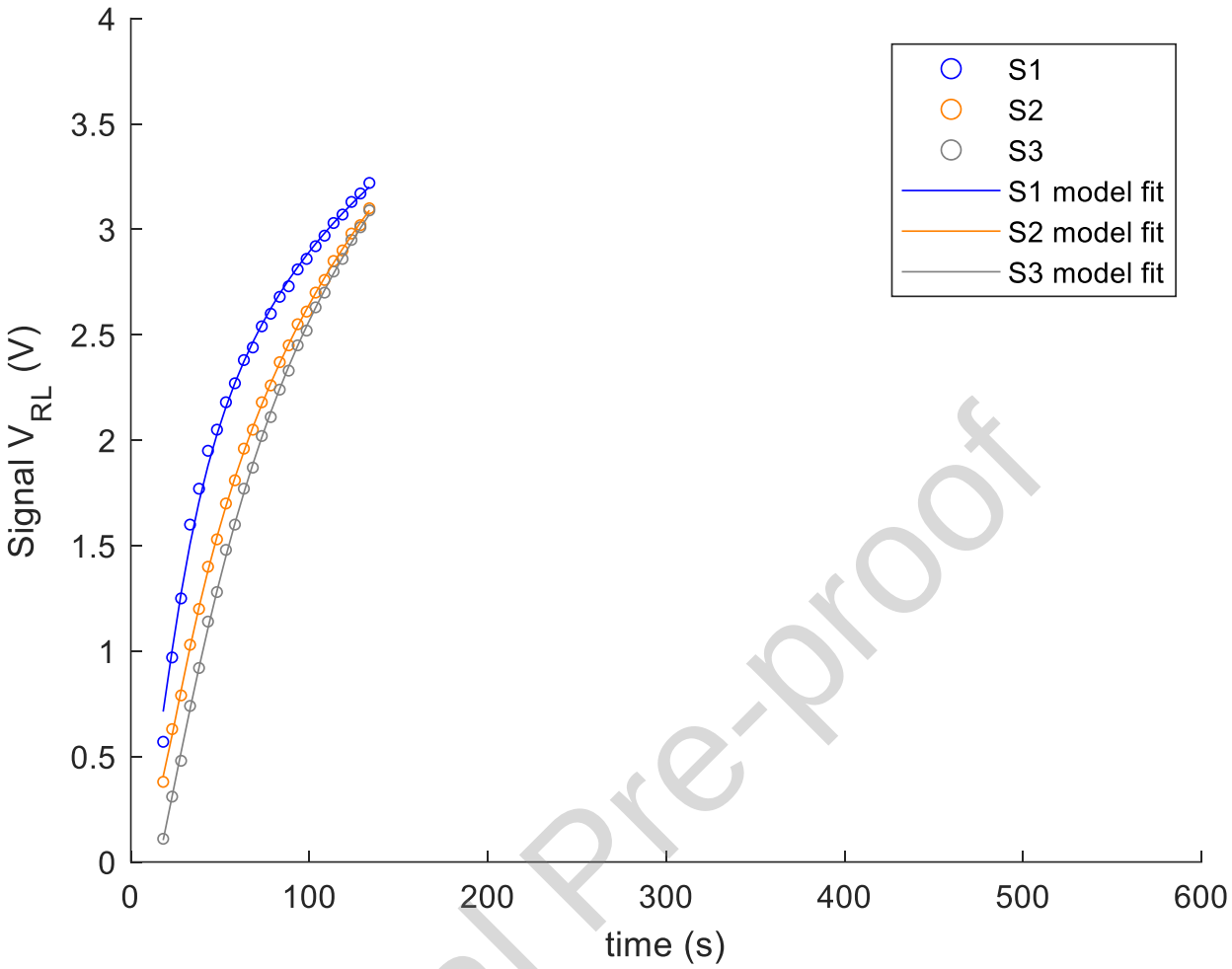

d)

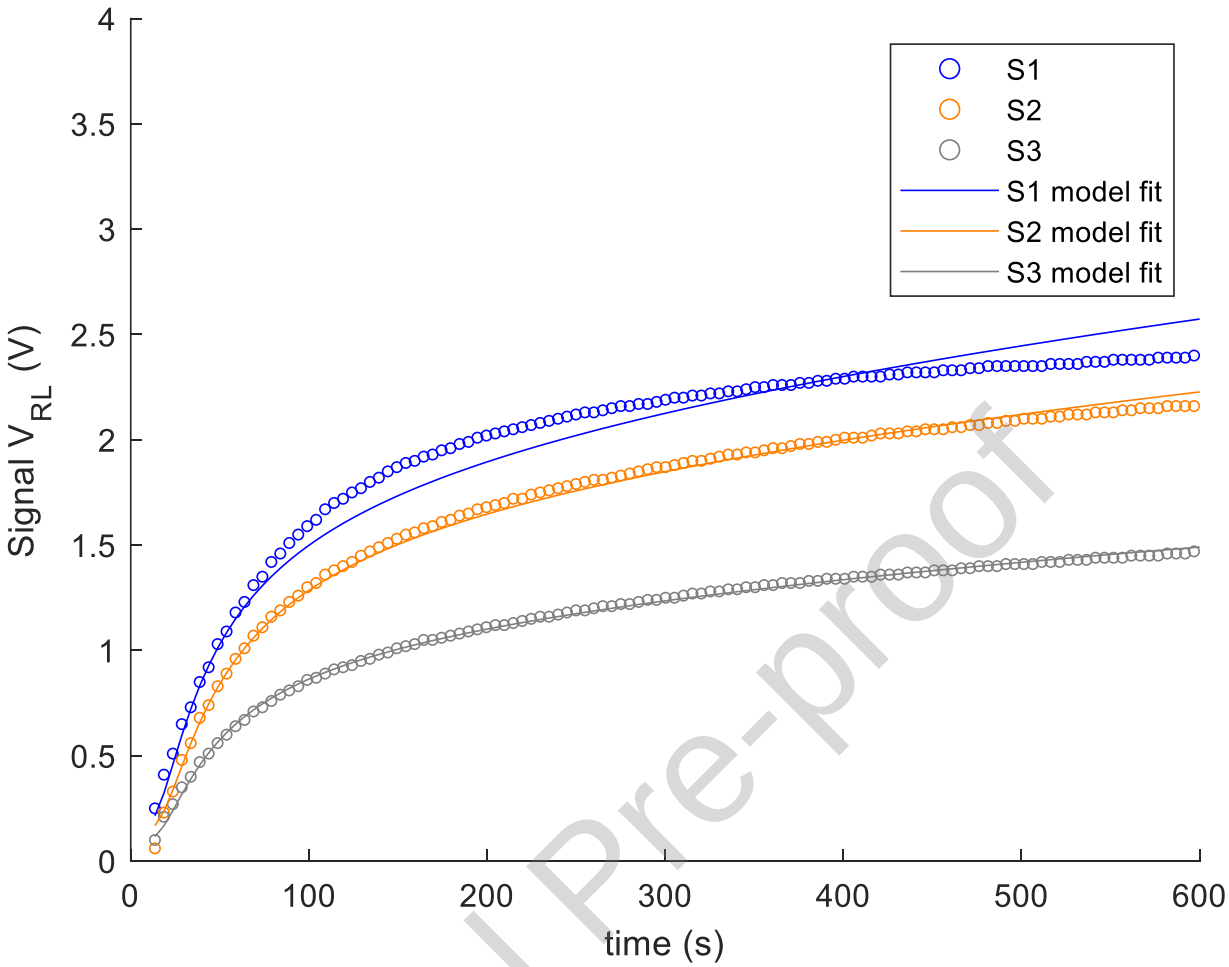

e)

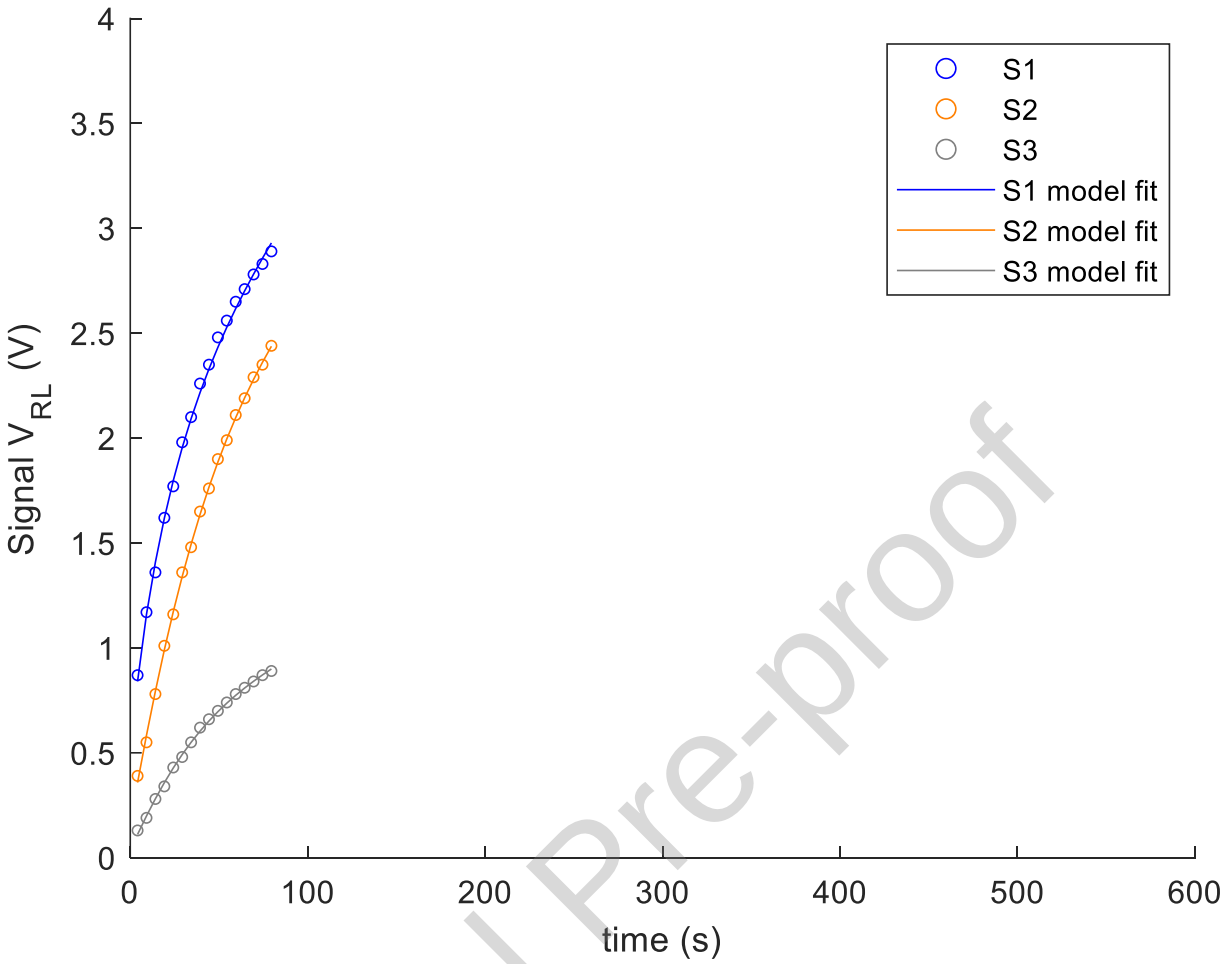

f)

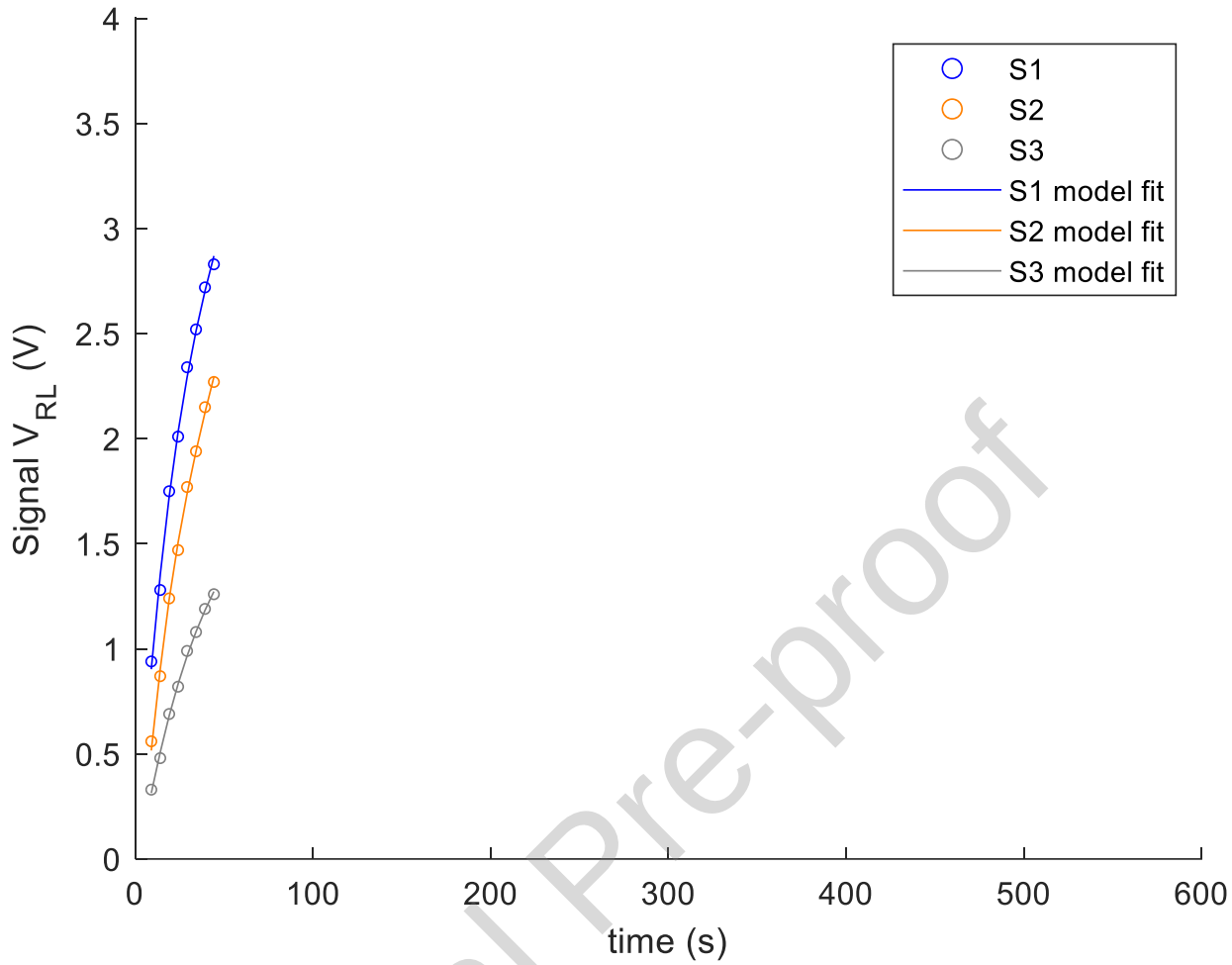

Fig. 12- Some examples of goodness of fitting to model for features extraction for a) TATP, b) acetone, c) hexane, d) formaldehyde, e) nitromethane and f) ethanol

a)

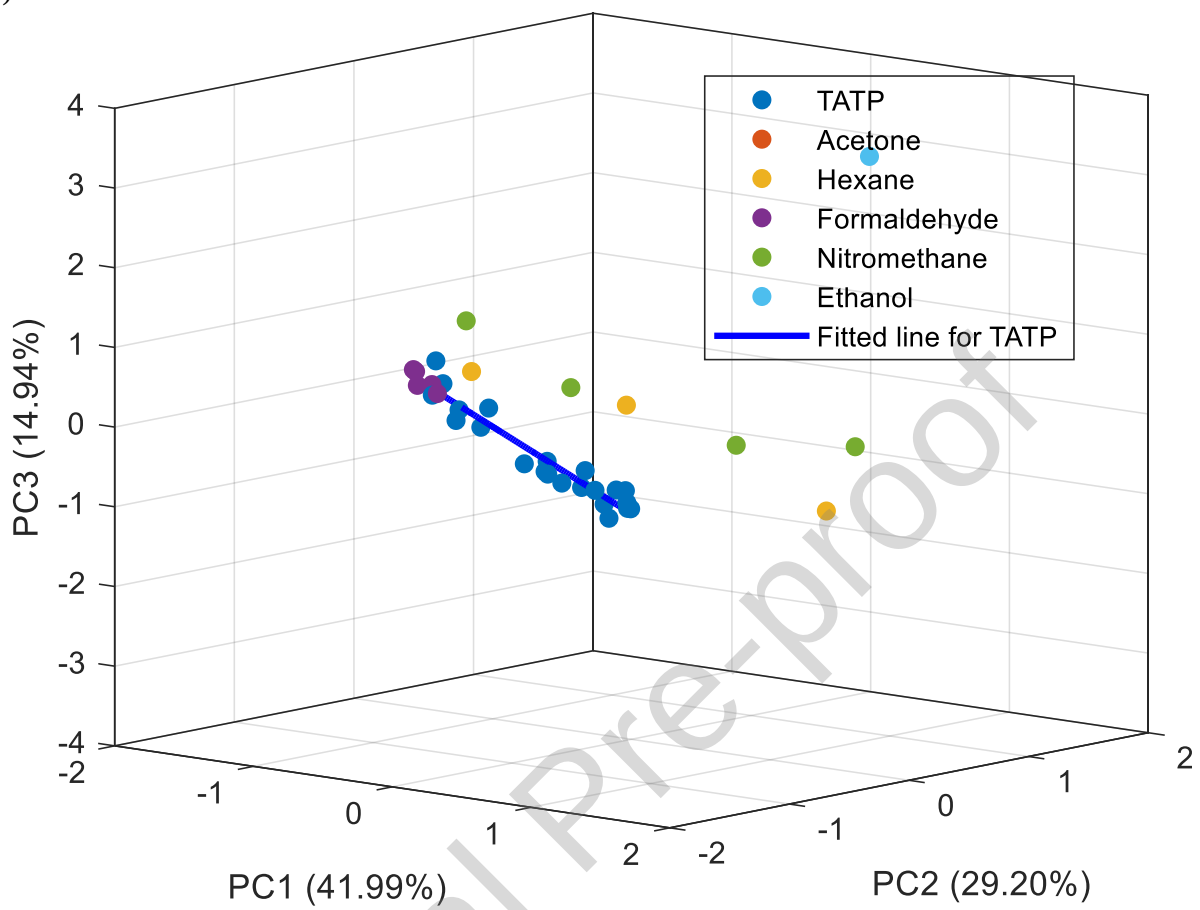

b)

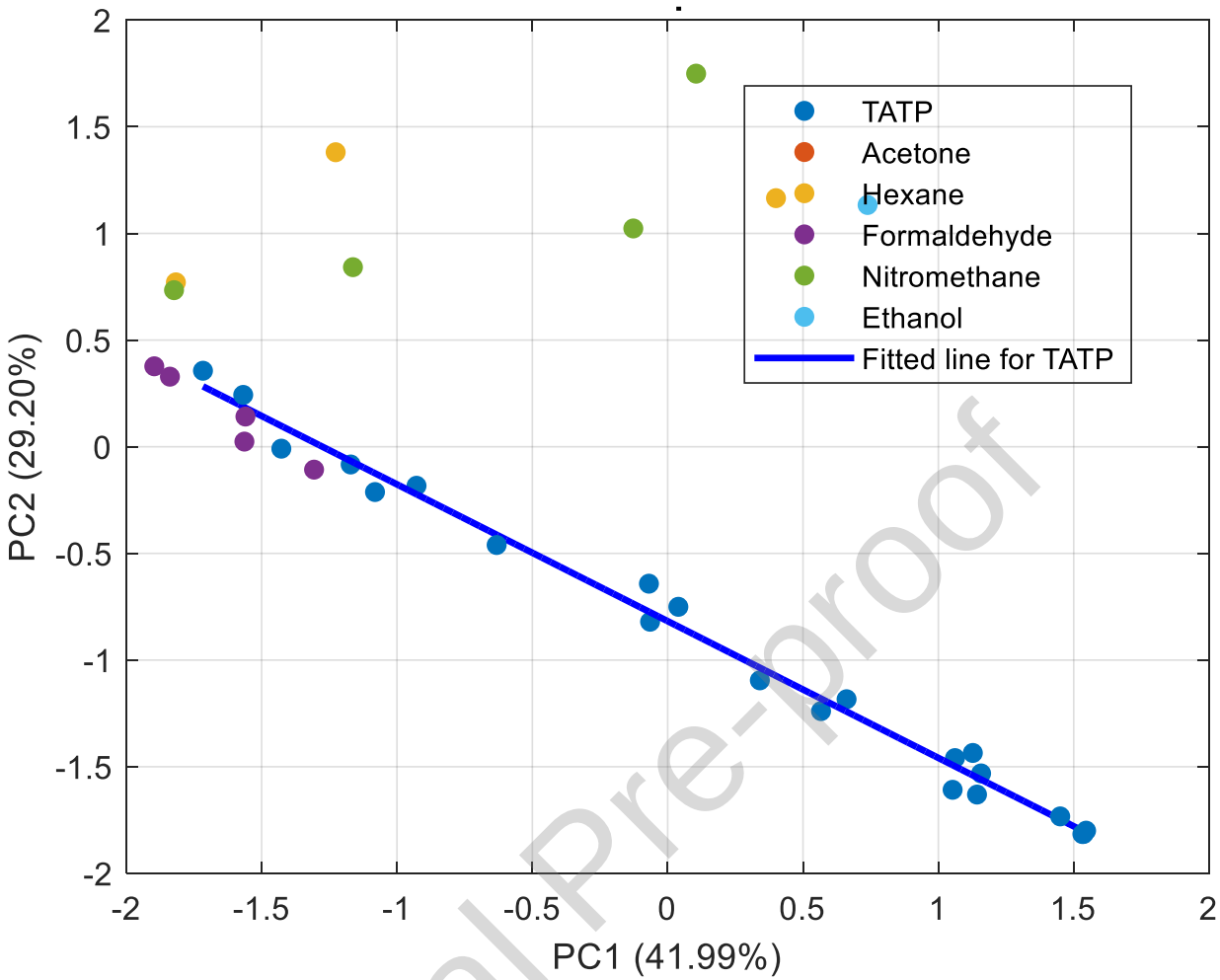

Fig. 13- PCA data analysis, a) 3D representation of first three principal components, b) PC1 vs PC2

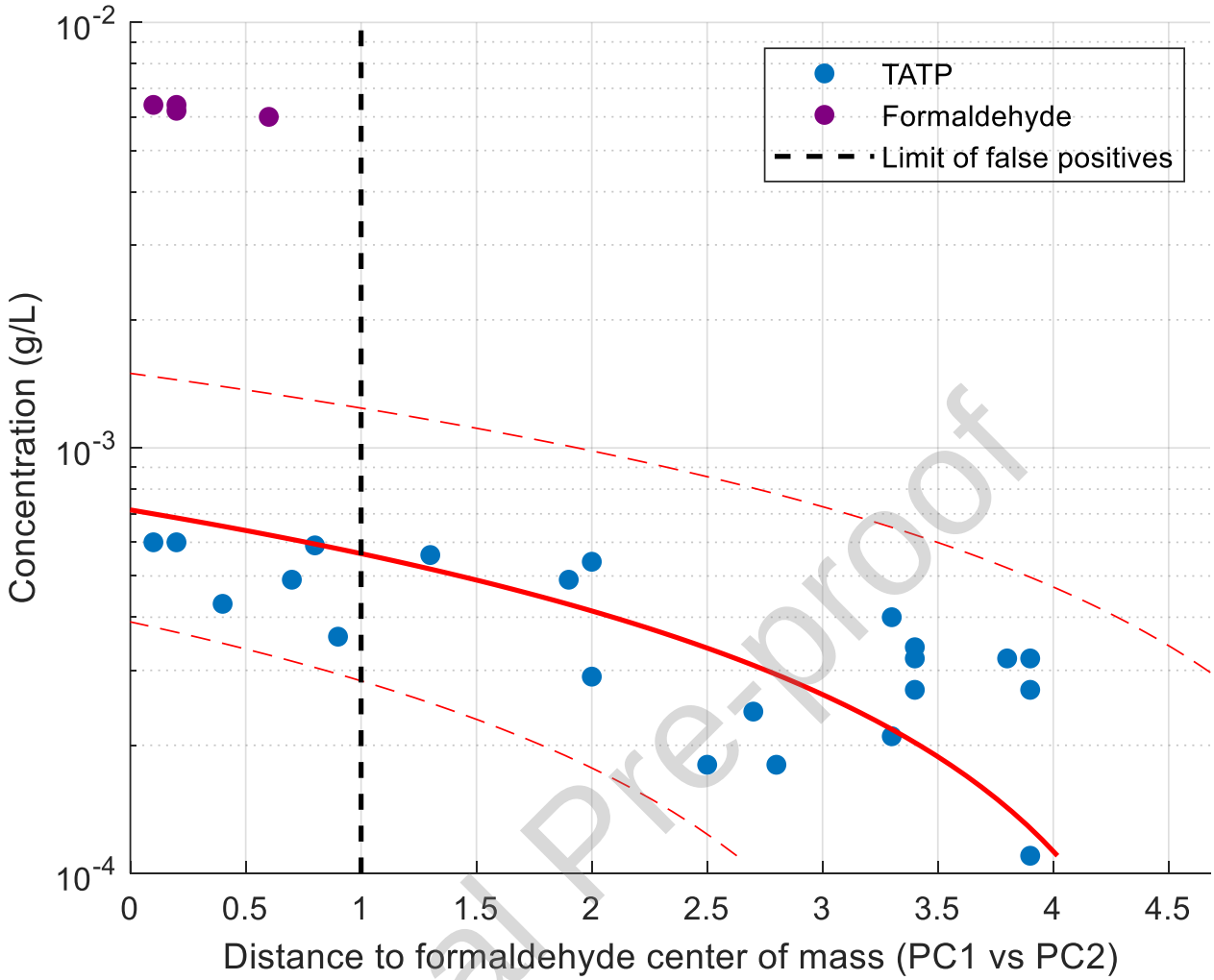

Fig. 14- Visualization of false positive identification of formaldehyde with region of TATP highly concentrated. Furthermore, it is observed a linear tendency in TATP concentration (confidence limits p=0.05) in PCA scattering.

Biographies

Raúl López has been a full-time researcher in energetic materials INTA since 2010 He received his BE and ME degree in Chemistry by University of Valladolid in 2001 and 2011 respectively. In addition, BE and PhD in Materials Engineering by University Rey Juan Carlos (Madrid) in 2014 and 2018 respectively. His current research work is focused on development of e-noses with security applications.

Marisol Vega is a full professor in Analytical Chemistry at the Universidad de Valladolid and member of the Institute of Sustainable Processes, with more than 30 years in research and

teaching. She has authored more than 70 research papers mainly focused on Electrochemistry, Chemometrics, Trace Analysis, Environmental Chemistry and Bioremediation.

Luis M. Deban is a full professor of Analytical Chemistry at the University of Valladolid with more than forty years of research in this field, close to seventy publications in international journals and a hundred communications to congresses. Currently Honorary Professor.

Rafael Pardo is a retired professor in Universidad de Valladolid with more than 45 years in Chemistry research and teaching. More than 100 research papers mainly focused on Electrochemistry, Environmental Chemistry and Chemometrics.

Declaration of Interest Statement
Conflict of interest
Authors declare no conflict of interest, because no professional judgement concerning a primary interest may be influenced by a secondary interest.

Funding source
Exclusive source of funding is INTA Project *ENASUS* declared in paper. No sponsors are involved in the study design, collection, analysis or interpretation of data. The writing of the manuscript and the decision to submit the manuscript for publication involved the second PhD of principal author.
No other activities related with a conflict of interests need to be considered

Highlights

- Innovative response model for Metal Oxide Semiconductor (MOS) sensors.
- Improved accuracy of vapor identification by Principal Component Analysis.
- Triperoxide Triacetone (TATP), Home-Made Explosive, identified by their vapor.
- Linearization of model features by MOS signal preprocessing in enoses.